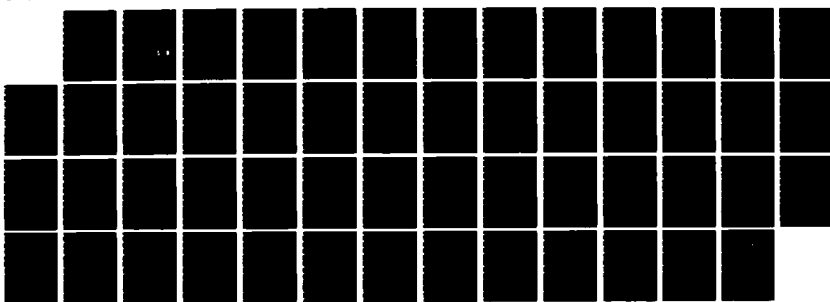


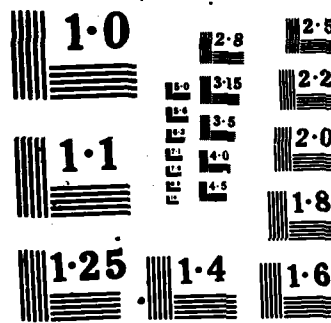
AD-A168 291 GEOMETRIC STRUCTURE PSEUDO BAND GRPS AND SURFACE  
VIBRATIONAL RESONANCES O. (U) CORNELL UNIV ITHACA NY

1/1

LAB OF ATOMIC AND SOLID STATE PHYSICS

UNCLASSIFIED M PERSSON ET AL. FEB 86 N00814-82-K-0576 F/G 28/12 NL





NATIONAL BUREAU OF S  
MICROCOPY RESOLUT TEST

AD-A168 291

12

SECURITY CLASSIFICATION OF THIS PAGE (When Data Entered)

REPORT DOCUMENTATION PAGE		READ INSTRUCTIONS BEFORE COMPLETING FORM
1. REPORT NUMBER	2. GOVT ACCESSION NO.	3. RECIPIENT'S CATALOG NUMBER
4. TITLE (and Subtitle)  Geometric Structure, Pseudo Band Gaps, and Surface Vibrational Resonances on Metal Surfaces		5. TYPE OF REPORT & PERIOD COVERED  Interim
7. AUTHOR(s) M. Persson, J.A. Stroscio, W. Ho		6. PERFORMING ORG. REPORT NUMBER  N00014-82-K-0576
9. PERFORMING ORGANIZATION NAME AND ADDRESS Laboratory of Atomic and Solid State Physics Cornell University, Clark Hall Ithaca, NY 14853-2501		10. PROGRAM ELEMENT, PROJECT, TASK AREA & WORK UNIT NUMBERS
11. CONTROLLING OFFICE NAME AND ADDRESS Office of Naval Research Washington, D.C.		12. REPORT DATE February, 1986
14. MONITORING AGENCY NAME & ADDRESS (if different from Controlling Office)		13. NUMBER OF PAGES 50
		15. SECURITY CLASS. (of this report)  Unclassified
		15a. DECLASSIFICATION/ DOWNGRADING SCHEDULE
16. DISTRIBUTION STATEMENT (of this Report)  Approved for public release; distribution is unlimited		
17. DISTRIBUTION STATEMENT (of the abstract entered in Block 20, if different from Report)		
18. SUPPLEMENTARY NOTES		
19. KEY WORDS (Continue on reverse side if necessary and identify by block number)		
20. ABSTRACT (Continue on reverse side if necessary and identify by block number)  It is shown by surface lattice dynamics that a new class of surface vibrational resonances arises in those frequency regions where there is a strong depletion in the bulk phonon density of states. The presence of these pseudo band gaps is due to the higher Fourier components in the phonon dispersion relations introduced by the particular coordination of atoms in layers parallel to the surface. This phenomenon is illustrated for the fcc (110) surfaces of Cu and Ni and bcc(111) surface of Fe. The pseudo band gap is found to be more pronounced for the longitudinal phonons propagating in		

DTIC  
ELECTED  
S JUN 04 1986 D

DTIC FILE COPY

DD FORM 1 JAN 73 1473

EDITION OF 1 NOV 65 IS OBSOLETE  
S/N 0102-014-66011

SECURITY CLASSIFICATION OF THIS PAGE (When Data Entered)

OVE

the bcc  $\{111\}$  than the fcc  $\{110\}$  directions due to the additional strong multiple interlayer forces arising from its geometric structure. A quantitative analysis based on surface lattice dynamics of the recorded electron energy loss spectra of Cu and Ni suggests that the surface interlayer force constant attains the same value as in bulk, and that the two outermost layers give the dominant contribution to the dipole activity. This resonance is found to exist throughout the  $\Gamma$ -X direction and makes an avoided crossing with a resonance derived from a band gap at the X-point. This novel dispersion behavior should be possible to observe by electron or atom scattering at larger parallel wavevector transfers.

Gamma-X

X

GEOMETRIC STRUCTURES, PSEUDO BAND GAPS, AND SURFACE VIBRATIONAL  
RESONANCES ON METAL SURFACES

M. Persson,<sup>†</sup> Joseph A. Stroscio,\* and W. Ho

Laboratory of Atomic and Solid State Physics  
and  
Materials Science Center  
Cornell University  
Ithaca, New York 14853

Abstract:

It is shown by surface lattice dynamics that a new class of surface vibrational resonances arises in those frequency regions where there is a strong depletion in the bulk phonon density of states. The presence of these pseudo band gaps is due to the higher Fourier components in the phonon dispersion relations introduced by the particular coordination of atoms in layers parallel to the surface. This phenomenon is illustrated for the fcc(110) surfaces of Cu and Ni and the bcc(111) surface of Fe. The pseudo band gap is found to be more pronounced for the longitudinal phonons propagating in the bcc [111] than the fcc [110] directions due to the additional strong multiple interlayer forces arising from its geometric structure. A quantitative analysis based on surface lattice dynamics of the recorded electron energy loss spectra of Cu and Ni suggests that the surface interlayer force constant attains the same value as in bulk, and that the two outermost layers give the dominant contribution to the dipole activity. This resonance is found to exist throughout the  $\bar{X}\bar{X}$  direction and makes an avoided crossing with a resonance derived from a band gap at the  $\bar{X}$ -point. This novel dispersion behavior should be possible to observe by electron or atom scattering at larger parallel wavevector transfers.

1985 PACS numbers: 68.30.+z, 63.20.-e, 79.20kz

MSC Report No. 5671

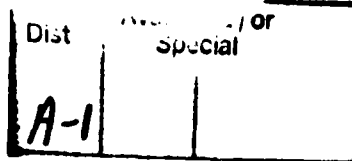
### 1. Introduction

The vibrational properties of clean metal surfaces have recently attracted a lot of attention both from an experimental and a theoretical point of view. These studies have been made possible by new surface sensitive vibrational spectroscopies such as inelastic He scattering and electron energy loss spectroscopy (EELS). These techniques probe vibrations with such high frequencies that the surface lattice dynamics cannot be described fully within the continuum elasticity theory. In this frequency regime the atoms vibrate with large relative displacements such that the surface geometric structure and the surface interatomic forces are expected to play a decisive role. Recent measurements on Ni(100) by EELS<sup>1</sup> and Ag(111) by inelastic He scattering<sup>2</sup> demonstrated that such information can be extracted from the surface vibrational spectra. An analysis of the EELS data recorded in the impact scattering regime has shown that the data can only be accounted for by a 20% increase of the surface force constant from the bulk value and a 3% contraction of the surface interlayer spacing.<sup>4</sup> On Ag(111) the presence of an anomalous peak in the measured spectra was shown in an analysis based on surface lattice dynamics to be a signature of a 50% reduction in the radial surface force constant from the bulk value.<sup>5</sup> Their analysis attributed this peak to be a surface resonance mode.<sup>5</sup>

The possibility to observe dipole active surface vibrational modes on clean metal surfaces was recently demonstrated for the (100) surfaces of Cu and Ni by EELS.<sup>6</sup> In a recent letter we reported the observation of dipole active resonance modes on the (110) surfaces of Cu and Ni.<sup>7</sup> These modes were shown from surface lattice dynamics calculations to be a new kind of

resonance arising from a pseudo band gap in the density of states for longitudinal phonons propagating normal to the surface. This gap defines a region where the bulk phonon density of states is strongly depleted and has a simple structural explanation in terms of the coordination of the atoms in the layers normal to the (110) direction of fcc crystals. No such gaps and resonances exist on fcc (100) or (111) surfaces.

This paper shows in detail for a few different cases how a surface vibrational resonance arises in situations with pseudo band gaps in the bulk phonon density of states. The surface is observed to split off a mode from the region of high density of bulk phonon states into the pseudo band gap region where the strong depletion of the density of states causes the mode to become a resonance. An argument is also given for explaining why the divergent van Hove singularities which are present in the bulk density of states disappear for a projection on the surface layers. These divergences disappear because an incident phonon at those frequencies interfere destructively with the phonons scattered from the surface. On the [110] surfaces of fcc Ni and Cu crystals the pseudo band gap is shown to exist along the  $\bar{\Gamma}\bar{X}$  direction in the surface Brillouin zone (SBZ). The corresponding surface vibrational resonance makes an avoided crossing with a resonance derived from a gap mode at the  $\bar{X}$ -point in the SBZ. This kind of phenomenon has, to the best of our knowledge, not yet been discussed in the literature. Previous lattice dynamical calculations for these surfaces<sup>14</sup> have shown that a surface vibrational resonance can develop when the surface splits off a mode from one bulk subband which becomes resonant with an overlapping second bulk subband. In contrast the resonances discussed in this paper are seen to result from a single bulk phonon band and possess a nonvanishing frequency at  $\bar{\Gamma}$ , the center of the



SBZ.

An extreme case of a pseudo band gap is found in the dispersion of longitudinal phonons in the [111] direction of body centered cubic crystals. In this case there exists two rather narrow surface resonances as illustrated for Fe(111). This analysis suggests in general that surface vibrational resonances should be observable on a variety of surfaces at points in the SBZ where a bulk phonon dispersion relation has a pseudo band gap.

A detailed quantitative comparison of the measured spectra with the calculated EEL spectra shows that the loss peak derived from the resonance is reproduced with a value for the surface force constant within  $\pm 15\%$  from its bulk value. This finding is rather remarkable in light of the large oscillatory relaxations of the surface layers observed by low energy electron diffraction (LEED) for these surfaces.<sup>8</sup> The spectra also give information about the dipole activity of the surface layers. The shape of the loss spectrum is well reproduced by only the two outermost surface layers giving the dominant contribution to the dipole activity. The dipole strength is found to be of the same order of magnitude as measured for the (100) surfaces.<sup>6</sup>

The vibrational structure of the surface appear in the measured spectra through a specific projection of the surface vibrational density of states. While the relevant projection probed in inelastic He scattering is essentially given by the displacements of the outermost surface atoms normal to the surface,<sup>9</sup> the relative rigid displacements of the surface layers is the relevant projection in inelastic dipole scattering.<sup>6</sup> Such vibrational density of states have been evaluated here from surface lattice dynamics for a semi-infinite substrate using simple force constant models.

The force constant models have been extracted from Born von Karman analysis of inelastic neutron scattering data with particular emphasis on the high frequency vibrations. The bulk phonon dispersions of Cu and Ni are well described by a single nearest neighboring force constant.<sup>10,11</sup> The dispersion of the longitudinal phonons in the [111] direction of Fe is more complex and requires at least 3 parameters.<sup>12</sup> The surface interlayer force constants have been chosen to have the same values as the bulk layers. This choice should be viewed as a reference model with no more justification than that it describes the large effect of the loss of coordination of atoms at the surface.

The surface vibrational density of states has been calculated using a Green function technique proposed by Lee and Joannopoulos.<sup>13</sup> This technique is based on the transfer matrix and its application to surface lattice dynamics is described in an appendix. Previous lattice dynamics calculations treating (110) surfaces of fcc crystals have been based on finite slabs,<sup>14</sup> where the surface resonance structure discussed here was not identified. A reinvestigation of these surfaces using the finite slab method<sup>15</sup> shows that this method is capable of identifying these resonances and is a convenient method for comparison to electron energy loss spectra where an instrumental energy broadening factor is required. However, the transfer matrix method for the semi-infinite crystal allows an exact determination of the spectral line shapes and is a more practical method for identifying very narrow resonances in the surface phonon density of states.

This paper is organized as follows. In Section 2 the experimental arrangement is described. A theoretical discussion is made in Section 3 to explain the origin of the pseudo band gaps and surface resonances.

Detailed comparison with experiments is given in Section 4, followed by a

discussion on the dispersion of the resonances in Section 5. The extension to bcc(111) surface is presented in Section 6. The paper is summarized in Section 7. The application of the transfer matrix method for calculating surface vibrational density of states is presented in the Appendix.

## 2. Experimental Details

The experiments were performed in a multitechnique ultrahigh vacuum system which is evacuated by turbomolecular, ion, and titanium sublimation pumps with a base pressure of  $4 \times 10^{-11}$  Torr.<sup>16</sup> The electron spectrometer is based on a double pass 127° cylindrical electrostatic deflector for the monochromator and analyzer. The scattering geometry is fixed with a total scattering angle of 120°. The angular acceptance of the analyzer is 1.8° at full-width-half-maximum (FWHM). The scattering plane containing the incident and scattered electrons is defined by the surface normal and the [110] crystallographic direction. The spectra were recorded in the specular direction at a temperature of 300 K. Impact energies of 3.2 and 4.3 eV were used for Cu and Ni respectively.

The samples, which were approximately 1 cm diam and 1 mm thick disks, were cleaned by neon ion bombardment (500 eV) and annealing to 750 and 1050 K for Cu and Ni respectively. The samples were spotwelded to a manipulator with a pair of 0.5 mm Ta wires for the Ni sample and with 0.5 mm Pt wires for the Cu sample. The clean surfaces displayed sharp 1×1 LEED patterns without any sign of typical impurity vibrations, such as O, C, or S, in the electron energy loss spectra. Similar procedure was used in preparing the Fe sample except that it was sputtered with 1 keV ions and annealed to 850 K. The most difficult contaminant to remove on the Fe surface was found to be oxygen. The Fe crystal was also mounted by two 0.5 mm Ta wires.

The vibrational spectra of the clean Cu and Ni(110) surfaces are shown in Fig. 1. The instrumental resolution is 4 meV FWHM. On both surfaces sharp loss features are observed within the bulk phonon bands at 20 and 24 meV for Cu and Ni respectively. Off-specular measurements show these losses to be excited by the dipole scattering mechanism.<sup>17</sup> Energy gain peaks are also observed with an intensity ratio to the energy loss peaks determined by the Bose-Einstein distribution factor at 300 K. An important feature of these losses is that the ratio of their energies scales as the ratio of the maximum bulk phonon frequency which is 29.7 and 36.7 meV for Cu<sup>10</sup> and Ni<sup>11</sup> respectively. This fact suggests that these losses are derived from longitudinal phonons propagating normal to the surface. A surface lattice dynamics analysis presented below shows in fact that the observed spectral features are due to a vibrational resonance, localized on the outer surface layers, which results from a split off state in a pseudo band gap in the density of states for longitudinal phonons propagating along the [110] direction.

### 3. Pseudo band gaps and resonances: fcc(110) surfaces

The notion of a pseudo band gap is illustrated by the dispersion of longitudinal bulk phonons in the [110] direction. A detailed analysis of the displacement fields for phonons scattered from the surface shows how a surface vibrational resonance can develop in this situation and why the divergent van Hove singularities present in the bulk phonon density of states disappear on the surface projection. The development of a resonance on the (110) surface is contrasted with the (100) and (111) surfaces where no such resonances appear.

For the (110) surface of fcc metals only rigid motions of the layers of atoms normal to the surface can be dipole active. Such a motion of the

bulk layers corresponds to longitudinal bulk phonons propagating in the [110] direction. It is known since the early studies by inelastic neutron scattering that the full bulk phonon dispersions for Cu and Ni can be well described by a Born-von Karman model of lattice dynamics based on central nearest neighboring force constants.<sup>10,11</sup> In this model the eigenvalue problem for the longitudinal bulk phonons propagating in the [110] direction is given by,

$$\omega^2 w_L = \frac{\alpha}{M} (4w_L - w_{L+1} - w_{L-1} - w_{L+2} - w_{L-2}), \quad (1)$$

and is in the [100] and [111] directions given by

$$\omega^2 w_L = \frac{2\alpha}{M} (2w_L - w_{L+1} - w_{L-1}), \quad (2)$$

where  $w_L$  is the displacement of an atom in the  $L$ th layer in a direction normal to the layer,  $\omega$  the frequency,  $\alpha$  the central nearest neighboring force constant, and  $M$  the mass of an atom.

From the translational symmetry of the bulk layers the solutions to Eqs. (1) and (2) are simple plane waves  $w_L = e^{i\pi\zeta L}$  with energies  $\omega(\zeta)$  satisfying the dispersion relation for the [110] direction,

$$\omega^2(\zeta) = \frac{\omega_0^2}{2} [\sin^2(\frac{\pi\zeta}{2}) + \sin^2(\pi\zeta)], \quad (3)$$

and for the [100] and [111] directions,

$$\omega^2(\zeta) = \omega_0^2 \sin^2(\frac{\pi\zeta}{2}), \quad (4)$$

where  $\omega_0^2 = 8\alpha/M$ . The resulting phonon dispersion from this simple force constant model for the lattice dynamics agrees fairly well with data from inelastic neutron scattering for all the major crystallographic directions as shown in Fig. 2 when  $\omega_0$  is adjusted so that  $\omega(\zeta=1)$  is equal to the measured value in the [110] direction, i.e.  $\omega(\zeta=1) = \omega_0/\sqrt{2}$ ,  $\omega_0 = 29.7$  and

36.7 meV for Cu and Ni, respectively. The fit is particularly good in the high energy region and the largest discrepancies are typically found in, for this analysis, the less interesting low energy region.

A characteristic feature of the dispersion in the [110] direction is its non-monotonic behavior with a maximum at  $\zeta = \zeta_m$ , well within the Brillouin zone. This behavior can be understood simply from the coordination of atoms in this direction shown in Fig. 3. In this case an atom has nearest neighbors not only in the nearest layer but also in the next nearest layer. The next nearest neighboring atom lies in the [110] direction and causes the next nearest interlayer force constant to be as strong as the nearest interlayer force constant in Eq. (1). This causes for instance the restoring force for the displacement fields at  $\zeta = 0.5$  to be stronger than at  $\zeta = 1.0$ . In the other two crystallographic directions an atom has only nearest neighboring atoms in the nearest neighboring layer and this causes the dispersion to be monotonic with  $\zeta$  as evidenced by Eqs. (2) and (4).

In surface vibrational spectroscopy one probes the vibrational density of states in the surface region. Before presenting results for the surface density of states we will consider first the density of states for a bulk layer. The phonon density of state  $g(\omega)$  for a bulk layer is simply determined by

$$g(\omega) = \sum_i \left| \frac{d\omega}{d\zeta} \right|^{-1} \Big|_{\zeta=\zeta_i} , \quad (5)$$

where the sum is over all positive  $\zeta_i$  satisfying  $\omega = \omega(\zeta_i)$ . From the phonon dispersion relations given by Eqs. (3) and (4)  $g(\omega)$  can be evaluated straightforwardly and is presented for Ni in Fig. 4 (upper panel). In the low energy limit  $\omega \approx c_s \zeta \pi / d$  and  $g(\omega)$  goes to a constant,  $g(\omega) = d/c_s \pi$ , where  $c_s$  is the longitudinal sound velocity and  $d$  the interlayer spacing.

The stationary points in the dispersion relation defined by  $\frac{d\omega}{d\zeta} = 0$  give rise to divergent van Hove singularities in  $g(\omega)$ .<sup>18</sup> In one-dimensional problems, as in the case considered here, the divergences are in most cases power singularities with an exponent  $-1/2$ . This kind of singular behavior is readily shown from the fact that it is possible to make a Taylor expansion  $\omega(\zeta) = \omega_c + \gamma(\zeta - \zeta_c)^2/2$  around an isolated stationary point  $\zeta = \zeta_c$  and Eq. (5) gives directly that

$$g(\omega) \approx \frac{1}{\sqrt{2|\gamma|}} |\omega - \omega_c|^{-1/2}, \quad \zeta \neq \zeta_c. \quad (6)$$

However, in some exceptional cases, which are not encountered here,  $\gamma = 0$  and the next leading term in the Taylor expansion gives rise to another value for the exponent. For metals it is also possible to have non-analytic behavior, Kohn anomalies, from the long-range interactions introduced by the sharp Fermi surface. These singularities are not discernible for Cu and Ni. The most important point to be made here about  $g(\omega)$  is the fact that the [110] dispersion relation has a relatively large density of states in a rather narrow region in  $\omega$ ,  $22 \leq \hbar\omega \leq 33$  meV, compared to the low energy region  $0 \leq \hbar\omega \leq 22$  meV. This latter region will for that reason be called a pseudo band gap. No such region can be defined for the other two directions [100] and [111].

In order to evaluate  $g(\omega)$  for a surface layer one needs a model for the effects of the surface on the force constants. An obvious effect of forming a surface is the corresponding loss of coordination of the surface atoms. Here we will only account for that effect on the interlayer force constant. The resulting equations describing the surface layers in

the [110] direction are given by,

$$\omega^2 w_1 = \frac{\alpha}{M} (2w_1 - w_2 - w_3) \quad (7)$$

$$\omega^2 w_2 = \frac{\alpha}{M} (3w_2 - w_1 - w_3 - w_4),$$

and for the outermost surface layers in the [100], [111] direction

$$\omega^2 w_1 = \frac{2\alpha}{M} (w_1 - w_2). \quad (8)$$

The presence of the surface breaks the translational symmetry and the solutions to Eqs. (1) and (7) can no longer be written as a single plane wave. Rather a wave  $e^{-i\pi\zeta L}$  incident on the surface will be reflected and can couple to another wave  $e^{+i\pi\zeta L}$  with the same energy  $\omega(\tilde{\zeta}) = \omega(\zeta)$ . This kind of argument suggests the following ansatz for the scattered wave in the [110] direction,

$$w_L = e^{-i\pi\zeta L} + R(\zeta) e^{i\pi\zeta L} + \tilde{R}(\zeta) e^{+i\pi\tilde{\zeta} L}. \quad (9)$$

This form for the ansatz is justified in the Appendix. Due to the non-monotonic behavior of the dispersion some care is needed to get the right boundary conditions. The reduced wavevector  $\zeta$  has to be choosen from the ranges  $-1 \leq \zeta < -\zeta_m$  and  $0 \leq \zeta < \zeta_m$  where the maximum in the phonon dispersion occurs at  $\pm \zeta_m$ . In these ranges the group velocity is positive,  $d\omega/d\zeta > 0$ , so that  $e^{-i\pi\zeta L}$  and  $e^{i\pi\zeta L}$  are incoming and outgoing waves, respectively. The other reflected wave  $e^{+i\pi\tilde{\zeta} L}$  is propagating for  $\omega/\omega_0 \geq 1/\sqrt{2}$  and similarly has to be choosen from the ranges where the group velocity is positive,  $d\omega/d\tilde{\zeta} > 0$ . For smaller energies  $\omega/\omega_0 < 1/\sqrt{2}$ ,  $\tilde{\zeta}$  is complex and  $e^{+i\pi\tilde{\zeta} L}$  is an evanscent wave and the sign of  $\text{Im}\tilde{\zeta}$  has to be chosen so that it is a decaying wave.

The two reflection coefficients  $R(\zeta)$  and  $\tilde{R}(\zeta)$  are now determined from the two equations of motion for the surface layers, Eq. (7). The two equations for  $R(\zeta)$  and  $\tilde{R}(\zeta)$  are given by,

$$d_i(\zeta)R(\zeta) + d_i(\bar{\zeta})\tilde{R}(\zeta) = -d_i(-\zeta) \quad i = 1, 2 \quad (10)$$

where

$$d_1(\zeta) = (v^2(\zeta) - 1/4) + \frac{1}{8}(e^{i\pi\zeta} + e^{i2\pi\zeta})$$

and

$$d_2(\zeta) = (v^2(\zeta) - 3/8) + \frac{1}{8}(e^{-i\pi\zeta} + e^{i\pi\zeta} + e^{i2\pi\zeta}).$$

Here  $v$  is the reduced energy  $v = \omega/\omega_0$ . The surface vibrational density of states defined as,

$$g(\omega) = \int_0^1 d\zeta |w_1|^2 \delta(\omega - \omega(\zeta)) \quad (11)$$

can now be evaluated from Eq. (9). It turns out, however, that it is more elegant and practical to evaluate  $g(\omega)$  by the transfer matrix method described in detail in the appendix. The resulting  $g(\omega)$  calculated by the transfer matrix method for the [110] direction is depicted in Fig. 4 (lower panel).

A noteworthy feature of  $g(\omega)$  is that the divergent van Hove singularities have disappeared in the projection on the outermost surface layer. This can be shown rather easily from Eqs. (9) and (10) to be due to the fact that one gets destructive interference between incident and reflected waves resulting in  $w_L \equiv 0$  at the stationary points. For instance at  $\zeta = \zeta_m$  the ansatz degenerates to,

$$w_L = (1 + \tilde{R}(\zeta_m))e^{-i\pi\zeta_m L} + R(\zeta_m)e^{+i\pi\zeta_m L}. \quad (12)$$

Instead of having two inhomogeneous equations for  $\bar{R}(\zeta)$  and  $R(\zeta)$  from Eq. (10) we have now two homogeneous equations for  $1 + \bar{R}(\zeta_m)$  and  $R(\zeta_m)$ . These two equations will in general have a trivial solution except in those accidental cases where the determinant is identically zero. Thus the contribution to  $g(\omega)$  from  $\zeta = \zeta_m$  is  $g(\omega) = |w_1(\zeta)|^2 / |\omega - \omega_m|$ . From Eq. (10) it is evident that  $w_1(\zeta)$  is analytic around  $\zeta = \zeta_m$ , and  $w_1(\zeta) = \lambda(\zeta - \zeta_m)$  since  $w_1(\zeta_m) = 0$ . Similarly for  $\omega(\zeta)$ ,  $\omega(\zeta) = \omega_m + \gamma(\zeta - \zeta_m)^2/2$ , and

$$g(\omega) = \frac{\sqrt{2}|\lambda|^2}{|\gamma|^{3/2}} (\omega_m - \omega)^{1/2}, \zeta \neq \zeta_m. \quad (13)$$

Thus the divergent van Hove singularity  $-(\omega - \omega_m)^{-1/2}$  at a bulk layer turns into a bounded van Hove singularity  $-(\omega - \omega_m)^{1/2}$  on a surface layer. This argument indicates also that the divergent van Hove singularity should not exist in  $g(\omega)$  for a projection on any layer for the semi-infinite substrate. A closer analysis reveals, however, that the bulk density of states are recovered in the limit  $L \rightarrow \infty$ . For instance, for a layer far inside,  $L \gg 1$ ,  $|w_L|^2 \approx 4\sin^2[\pi(\zeta - \zeta_m)L]$  when  $\zeta \neq \zeta_m$ . Thus  $g(\omega)$  will rise rapidly when going away from  $\omega_m$  and have a large maximum  $8L/|\gamma|$  at  $\zeta - \zeta_m = 1/2L$ , arbitrarily close to  $\omega_m$ . This argument for the disappearance of the divergent van Hove singularities in a projection of  $g(\omega)$  on a surface layer can be shown to apply to more general situations. For instance, it is not necessary that surface force constants are the same as in the bulk region.

Most importantly,  $g(\omega)$  shows a sharp narrow feature around 23 meV as seen in Fig. 4 (lower panel). This feature is now shown to be a surface vibrational resonance. In a situation when there is an absolute band gap it is well known that the surface can introduce a localized state split off

from the band. In this case there is no absolute band gap rather a pseudo band gap. The surface can possibly split off a state from the band which turns into a resonance by overlapping with the low density of bulk states in the pseudo band gap. This expectation is confirmed from an analysis of the reflection coefficient for  $\omega/\omega_0 < 1/\sqrt{2}$ ,  $\zeta = 1 + i\kappa$  where

$\cosh \pi \kappa = \frac{1}{4} [1 + \sqrt{25 - 32(\omega/\omega_0)^2}]$  and the complex part gives rise to an evanescent wave  $(-1)^L e^{-\kappa L}$ . The corresponding reflection coefficient  $\tilde{R}(\zeta)$  is found to have a simple pole for complex  $\nu$  at

$\nu_{\text{pole}} = 0.663 + i0.047$  (for Ni,  $\nu_{\text{pole}} = (24.3 + i1.73)\text{meV.}$ ) The existence of such a pole with an imaginary part  $\omega_I$  relatively close to the real axis justifies calling this rather sharp peak a surface vibrational resonance. Note that the peak is quite asymmetrical due to interference with bulk states in the depicted projection, a feature which is typical for Fano-resonances.<sup>19</sup>

For the [100] and [111] directions the ansatz for the solution to Eqs. (2) and (8) has a more simple form

$$w_L = e^{i\pi\zeta L} + R(\zeta)e^{-i\pi\zeta L} \quad (14)$$

for  $0 < \zeta < 1$ . This ansatz inserted into Eq. (8) for the surface layer gives a simple form for the reflection coefficient  $R(\zeta) = e^{i\pi\zeta}$ . As a function of  $\nu$  this reflection coefficient,  $R(\nu) = 1 - 2\nu^2 + 2i\sqrt{\nu^2 - \nu^4}$  (when  $0 < \zeta < 1$ ), has no poles associated with any resonances. The phonon density of states  $g(\omega)$  projected on a surface layer can now be evaluated directly from Eq. (11) and is given by,

$$g(\omega) = \frac{4}{\pi} \sqrt{1 - \left(\frac{\omega}{\omega_0}\right)^2}. \quad (15)$$

This density of states shows accordingly no surface vibrational resonances

as depicted in the lower panel of Fig. 4.

#### 4. Comparison with experiment

An attractive feature of EELS is the possibility to analyze quantitatively measured dipole active losses.<sup>20</sup> The dipole loss function for longitudinal bulk phonons is calculated for Ni and compared with the measured spectrum. The sensitivity of the calculated spectra to changes in the surface force constant and the distribution of the dipole activity among the surface layers are also investigated.

In a recent letter it was shown both experimentally and theoretically that the displacements of the outer layers of metal atoms can give rise to a long range dipole field due to incomplete screening by the conduction electrons of the electric field from the displaced ion cores.<sup>6</sup> The strength of the dipole field is described by effective charges  $e_L^*$  which relate the normal component of the dynamic dipole moment  $\mu_z$  to the rigid displacements  $w_L$  of layer L normal to the surface through,

$$\mu_z = \sum_L e_L^* w_L. \quad (16)$$

Here we use the same model for  $e_L^*$  as in Ref. 6,

$$e_1^* = -e_2^* = e^* \text{ and } e_L^* = 0, L > 2. \quad (17)$$

Note that a rigid displacement of the metal atoms normal to the surface cannot give rise to a dipole moment. i.e.  $\sum_L e_L^* = 0$ . The projection of the phonon density of states relevant for dipole losses is accordingly given by,

$$g(\omega) = \int_0^1 dz \left| \sum_L n_L^* w_L(z) \right|^2 \delta(\omega - \omega(z)) \quad (18)$$

where  $n_L^* = e_L^*/e_{tot}^*$ , with  $e_{tot}^* = (\sum_L e_L^{*2})^{1/2}$ , is the normalized field of

effective charges. The spectral function  $S(\omega)$  for the dipole-dipole correlation function appearing in the energy loss function is related to  $g(\omega)$  through,<sup>21</sup>

$$S(\omega) = (1 + n(\omega)) e_{\text{tot}}^{*2} \frac{\hbar}{2M\omega} g(\omega), \quad (19)$$

where the mass  $M$  of a metal atom appears in the root-mean-square amplitude  $\hbar/2M\omega$  for phonons with energy  $\hbar\omega$  and  $n(\omega)$  is the Bose-Einstein distribution factor.

From inelastic dipole scattering theory the inelastic current  $I_1(\omega)$  of electrons collected in the detector around the specular direction after experiencing an energy loss  $\hbar\omega$  is given with sufficient accuracy by,<sup>20</sup>

$$I_1(\omega)/I_{\text{tot}} = \frac{\pi m e^2}{\hbar^2 A E_0 \cos \alpha} f(E_0, \omega, \alpha) S(\omega), \quad (20)$$

where  $I_{\text{tot}}$  is the total integrated intensity of the elastic peak in the energy loss spectrum,  $m$  the electron mass,  $A$  the area of the surface primitive cell, and  $E_0$  the kinetic energy of the electron incident with an angle  $\alpha$  from the surface normal. The function  $f(E_0, \omega, \alpha)$  is given by,<sup>20</sup>

$$f(E_0, \omega, \alpha) = (\sin^2 \alpha - 2\cos^2 \alpha) Y + (\sin^2 \alpha + 2\cos^2 \alpha) \ln X, \quad (21)$$

where  $Y = \theta_1^2/(\theta_1^2 + \theta_0^2)$ ,  $X = (\theta_0^2 + \theta_1^2)/\theta_0^2$ ,  $\theta_0 = \hbar\omega/2E_0$  gives the angular extension of the dipole lobe, and  $\theta_1$  the half-angle of the detector aperture. The loss function depicted in Fig. 5 is now obtained from Eq. (20) by calculating the projected phonon density of states defined in Eq. (18) by the transfer matrix method for the distribution of effective charges given in Eq. (17). The parameters  $\alpha$ ,  $\theta_1$ , and  $E_0$  are determined from the experimental conditions described in Section 2, and the experimental resolution was introduced by a 4 meV Gaussian broadening of  $g(\omega)$ . The total effective charge  $e_{\text{tot}}^*$  had to be chosen to be 0.034e and

0.039e for Cu and Ni, respectively, in order to reproduce the measured loss intensities at 300 K. These values are of the same order of magnitude as for the value determined previously for the Cu(100) surface.<sup>6</sup> Because the resonance gives rise to a rather sharp loss peak there has been no particular need to have a detailed analysis of the contribution from the electron-hole pair excitations to subtract the background.<sup>22</sup>

The calculated position of 24.5 meV and the peak width of 6 meV for the surface vibrational resonance shown in Fig. 5 are in good agreement with the measured values for Ni. Note that the value for this peak position is about 1 meV higher than for the peak position deduced from  $g(\omega)$  for the projection on the outermost layer. This difference is due to the fact that the low energy bulk phonons contribute much less to this dipole active projection, which suppresses the asymmetry of the peak. The peak position is thus closer to the value for the real part of the pole in the complex  $\omega$ -plane as given in the previous section. For Cu,  $g(\omega)$  is obtained in the advocated force constant model simply by scaling the phonon energies with  $\omega_0(\text{Cu})/\omega_0(\text{Ni}) \approx 0.81$ . This gives an energy of 19.8 meV, in good agreement with the measured value of 20 meV observed in Fig. 1.

There are no reasons to expect that the only effect of the surface is the loss of coordination of atoms in the surface region as described by Eq. (7). For instance, both model calculations for the total energy<sup>23</sup> and low energy electron diffraction (LEED)<sup>8</sup> measurements have shown that the atoms relax oscillatorily in the surface region for many metals. In these new equilibrium positions for the atoms the force constants can be different from the bulk values. Off-specular measurements of the Rayleigh surface phonon dispersion on Ni(100) by EELS have suggested that the interlayer force constant between the first and second layer is about 20%

larger than the bulk value.<sup>1,4</sup> On Ag(111) the observation by inelastic He scattering of a surface vibrational resonance away from the  $\bar{\Gamma}$ -point in the SBZ could be accounted for by a reduction of about 50% of the radial part of the force constant between atoms in the surface region.<sup>2,5</sup>

The position of the surface vibrational resonance observed in the energy loss spectrum in Fig. 1 should also contain information about surface force constants. The sensitivity of the position of the resonance to changes in the surface interlayer force constants has been investigated by calculating a dipole active projection of the phonon density of states  $g(\omega)$  for different values of the surface interlayer force constants for Ni. There are several conceivable ways to modify surface force constants and we have chosen to modify the surface force constant between atoms in the outermost layer and their nearest neighboring atoms in the second and third layer. The modification is described by the following equations of motion for the surface layers,

$$\begin{aligned}\omega^2 w_1 &= \frac{\alpha_s}{M} (2w_1 - w_2 - w_3) \\ \omega^2 w_2 &= \frac{\alpha_s}{M} (w_2 - w_1) + \frac{\alpha}{M} (2w_2 - w_3 - w_4) \\ \omega^2 w_3 &= \frac{\alpha_s}{M} (w_3 - w_1) + \frac{\alpha}{M} (3w_3 - w_2 - w_4 - w_5).\end{aligned}\tag{22}$$

The resulting phonon density of states is shown in Fig. 6 (upper panel) for three different values of  $\alpha_s/\alpha$ . A 25% increase and decrease of  $\alpha_s$  relative to  $\alpha$  shifts the peak upwards by 1.8 meV and downwards by 2.7 meV, respectively. The experimental resolution is such that it can determine the peak position within 1 meV and could accordingly detect changes of  $\alpha_s$  within about  $\pm 15\%$  relative to  $\alpha$ . There are also notable changes in the

width of the resonance when  $\alpha_s$  is changed. It narrows and widens with about a factor of 2 when  $\alpha_s$  is increased and decreased by 25% relative to  $\alpha$ , respectively. The width of the calculated loss peak is close to the measured width which also supports the range of surface interlayer force constant  $\alpha_s$  suggested by the peak position.

Another consideration to be taken into account is how the effective charges are distributed among the surface layers. In the case of the Cu(100) surface the results from a jellium model calculation for Cu suggested the distribution defined in Eq. (17).<sup>6</sup> The application of the same model for the Cu(110) surface gives, however, that even the third and fourth layers have an appreciable effective charge  $e_L^*$  mainly due to a smaller interlayer distance in this direction. In Fig. 6 we present results for  $g(\omega)$  calculated for Ni with two different distributions for  $n_L^* = e_L^*/e_{tot}^*$  extending to the third and fourth layers and compare with the result from the distribution defined in Eq. (17). For the other two distributions the resonance peak is still prominent but the strength of the states in the upper bulk band region has been appreciably enhanced. The measured loss spectra for Cu and Ni shown in Fig. 1 do not indicate such a strong contribution from the bulk states.

Thus our analysis of the loss spectra suggests that there are no dramatic changes in the surface interlayer force constants from the bulk values. Further the data favor the model that the effective charges are dominant for the two outermost surface layers.

##### 5. Dispersion of the resonance along the $\bar{\Gamma}$ -X direction

The dispersion of surface vibrational modes along different directions in the SBZ has been shown to be feasible to measure for a few metal

surfaces by inelastic He scattering<sup>2,3</sup> and off-specular EELS.<sup>1</sup> Therefore it is of interest to know how the resonance disperses away from the  $\bar{\Gamma}$ -point. It is found that the resonance exists and is derived from a pseudo band gap even out to the  $\bar{X}$ -point. The resonance makes an avoided crossing with another resonance derived from a surface phonon in a bulk band gap. Close to the  $\bar{X}$ -point the resonance leaves the bulk subbands and appears as a surface phonon.

Along the  $\bar{\Gamma}$ - $\bar{X}$  direction the displacements of the atoms partition into two classes due to the reflection plane symmetry. The odd modes are polarized in the y-direction and are symmetry forbidden to couple with displacements of atoms polarized in the x-z plane which form the even class. In the nearest neighboring central force constant model the motion of atoms in the y-direction gives rise to a monotonic dispersion of the corresponding phonons with no pseudo band gaps. Henceforth the y-motion will not be considered further. The equations of motion for displacements of atoms in the x-direction and in the z-direction are coupled along the  $\bar{\Gamma}$ - $\bar{X}$  direction and are for the bulk layers given by,<sup>25</sup>

$$\begin{aligned}\omega^2 u_L = \frac{\alpha}{M} & [(4-2\cos(\pi\xi))u_L - \cos(\pi\xi/2)(u_{L-1} + u_{L+1}) \\ & + i\sin(\pi\xi/2)(w_{L+1} - w_{L-1})],\end{aligned}\tag{23}$$

$$\begin{aligned}\omega^2 w_L = \frac{\alpha}{M} & [4w_L - \cos(\pi\xi/2)(w_{L+1} + w_{L-1}) - (w_{L+2} + w_{L-2}) \\ & + i\sin(\pi\xi/2)(u_{L+1} - u_{L-1})],\end{aligned}$$

where  $u_L e^{ik_x R_x}$  and  $w_L e^{ik_x R_x}$  are displacements in the x- and z-directions, respectively, of an atom at position  $\vec{R}$  in Layer L, and  $\xi = k_x a / \sqrt{2\pi}$  is the reduced wavevector along the  $\bar{\Gamma}$ - $\bar{X}$  direction. At the  $\bar{\Gamma}$ -point ( $\xi=0$ ) the equations of motion for  $u_L$  and  $w_L$  are decoupled and Eq. (1) is

recovered for  $w_L$ .

The solutions to Eq. (23) are plane waves  $u_L = u(\xi, \zeta) e^{i\pi\xi L}$  and  $w_L = w(\xi, \zeta) e^{i\pi\xi L}$  which would result in two branches of the dispersion relation, one lower  $\omega_L = \omega_L(\xi, \zeta)$  and one upper  $\omega_U = \omega_U(\xi, \zeta)$ . The behavior of these two branches at  $\xi=0.6$  is illustrated in Fig. 7. If one artificially removes the coupling between  $u_L$  and  $w_L$  then the dispersion for phonons polarized in the x-direction is monotonic and crosses twice the dispersion for phonons polarized in the z-direction. The latter dispersion is non-monotonic due to the strong coupling to the second nearest layer. The coupling present in Eq. (23) between  $u_L$  and  $w_L$  causes these two branches to make two avoided crossings with corresponding interchange of character and makes them both non-monotonic with  $\zeta$ .

The influence of the surface on the force constants is modelled in the same way as in Section 3 by taking into account only the loss of coordination of atoms in the surface region. In this complex case we will not attempt to write out the form of the scattered wave for an incident wave. It is much more tractable to generate results for the surface vibrational density of states by using the transfer matrix method. This method cannot be applied directly to this system, however, due to the fact that the dynamical submatrix  $D_{01}$  between the principal layers is singular (see Appendix). This matrix  $D_{01}$  can be regularized, however, by introducing a small second layer coupling  $\frac{a}{M} r(u_{L+2} + u_{L-2})$  into the equations of motion for  $u_L$  in Eq. (23). The value of  $r=0.01$  is found to be sufficiently small for an accurate calculation of the phonon density of states. This value for  $r$  is much smaller than the errors in the nearest neighboring force constant model used to describe Cu and Ni.

The results in Fig. 7 for the phonon density of states  $g(\omega, \xi)$  at  $\xi=0.6$

projected on the x-motion and the z-motion of the outermost layer show several prominent features. There is a localized state in the gap at 11.1 meV, the surface phonon  $S_1$  in the notation of Ref. 14, being split off from the bulk subbands by the reduction of the restoring forces in the surface region. The x-projection of  $g(\omega, \xi)$  shows a narrow peak at 24 meV just below the minimum energy of the upper branch which can be interpreted as a state being split off from the upper branch and turning into a resonance due to overlap with states in the lower branch. Thus the origin of this resonance is the same as for the resonance discussed in the work on Ag(111) where an "anomalous" peak was observed in inelastic He scattering.<sup>2</sup> There is, however, another narrow peak in the z-projection of  $g(\omega, \xi)$  around 19 meV. The non-monotonic behavior of the lower branch suggests the interpretation that this peak is a resonance derived from the corresponding pseudo band gap of the lower branch below  $\omega_L(\xi, \zeta=1)$ . The upper branch shows similar non-monotonic behavior with a pseudo band gap in between  $\omega_{u,\min}$  and  $\omega_u(\xi, \zeta=1)$  which results in a resonance at 31.1 meV, very close to  $\omega_u(\xi, \zeta=1)$ . However, its dominant amplitudes are on layers further inside the surface.

By calculating the x- and z-projections of  $g(\omega, \xi)$  on the outermost layer for several values of  $\xi$  between 0 and 1 the behavior of the surface vibrational modes can be followed along the  $\bar{\Gamma}-\bar{X}$  direction as shown in Fig. 8. At the  $\bar{X}$ -point we have three surface phonons for displacements polarized in the x-z plane (i)  $S_1$  the Rayleigh surface phonon (ii)  $S_0$  which exists only close to  $\bar{X}$  and (iii)  $S_7$  a gap mode. The labelling of the modes are taken from the work by Allen, Alldredge and DeWette<sup>14</sup> except for  $S_0$  which was not identified in their slab calculations. The mode  $S_0$  is localized on the second and third layer and is predominantly polarized in

the z-direction. This mode turns into a resonance  $MS_0$  inside the lower bulk subband and lies in the pseudo band gap just below  $\omega_L(\xi, \zeta=1)$ . At around  $\xi=0.5 - 0.6$  the resonance interacts with the  $MS_7$  resonance and makes an avoided crossing with a corresponding interchange of character. The resonance  $MS_7$  is a continuation of the gap mode  $S_7$  into the bulk subbands and becomes mainly polarized in the x-direction for  $0.6 < \xi \leq 1.0$ . When  $\xi$  approaches the  $\bar{\Gamma}$ -point ( $\xi=0$ )  $MS_7$  goes over into the resonance discussed in previous sections and is mainly polarized in the z-direction. From the  $\bar{\Gamma}$ -point to the avoided crossing the width of  $MS_7$  remains roughly the same (about 3.5 meV) and after it interchanges character it sharpens appreciable to a width less than 0.5 meV.  $MS_0$  broadens and gets more localized on the outermost layer away from the  $\bar{\Gamma}$ -point and just at the crossing the width is about 2 meV. After the crossing the width remains about the same and sharpens up only just before leaving the bulk subband. Thus at the crossing the widths of the resonances overlap, which makes the avoided crossing less well defined.

#### 6. An extreme case: The bcc(111) surface

Non-monotonic phonon dispersion relations are not only found in the [110] direction of fcc metals but exists also in the [111] direction of bcc metals.<sup>24</sup> In general the phonon dispersion relations in cubic crystals can be written in terms of a Fourier series in the interlayer force constants due to factorization of the dynamical matrix. The higher Fourier components result from additional interlayer coupling which leads to non-monotonic dispersion relations. In the particular case of Fe(111) the longitudinal phonon dispersion relation shows an additional extreme as a result of more extensive multiple interlayer couplings. This leads to a

pseudo band gap that is more pronounced than on the fcc(110) surface. The multiple extremes are found to give rise to two sharp surface vibrational resonances.

In the [111] direction of a monoatomic bcc crystal an atom has nearest neighboring atoms not only in the nearest layer but also in the third nearest layer (Fig. 9). While second nearest neighboring atoms only appear in the second nearest layer. It is well known from studies by inelastic neutron scattering that it is not sufficient to consider only nearest neighboring force constant models as expected from the fact that the distances  $a$  and  $\sqrt{3}a/2$  to the nearest and second nearest neighboring atoms, respectively, are rather close ( $a$  is the lattice constant).<sup>12</sup>

The analysis of the experimental data in terms of a general tensor force constant model shows dominant interactions to reach second nearest neighboring atoms. Thus by retaining only up to second nearest neighboring force constants the eigenvalue problem for longitudinal phonons in the [111] direction is given by,

$$\begin{aligned} M\omega^2 w_L = & (8\alpha_1 + 2\alpha_2 + 4\beta_2)w_L \\ & - (3\alpha_1 - 2\beta_1)(w_{L+1} + w_{L-1}) \\ & - (\alpha_2 + 2\beta_2)(w_{L+2} + w_{L-2}) \\ & - (\alpha_1 + 2\beta_1)(w_{L+3} + w_{L-3}), \end{aligned} \quad (24)$$

where  $w_L$  is the rigid displacement of a bulk layer  $L$  in the [111] direction, and  $\alpha_1$ ,  $\beta_1$  and  $\alpha_2$ ,  $\beta_2$  are the first and second nearest neighboring force constants. The values for these force constants are taken directly from experimental data,<sup>12</sup>  $\alpha_1/m = 78.89$  (meV)<sup>2</sup>,  $\beta_1/m = 68.38$  (meV)<sup>2</sup> and  $\alpha_2/m = 70.15$  (meV)<sup>2</sup> and  $\beta_2$  is about 30 times smaller and is neglected here. The deviations of this tensor force field

from a central force field where  $\alpha_1 = \beta_1$  and  $\beta_2 = 0$  are rather small. Using this force constant model the dispersion of the longitudinal phonons,  $w_L = e^{i\pi\zeta L}$ , agrees well with the experimental data, as seen in Fig. 10. The most apparent discrepancy is around 7% between the model and the data and is found at the second extreme. The existence of two extremes within the zone boundary is due to the strong coupling to the third layer introduced by the presence of a nearest neighboring atom in that layer in the [111] direction.

As expected from the non-monotonic dispersion relation in Fig. 10, the phonon density of states projected on a bulk layer has a pseudo band gap in the region  $0 \leq \hbar\omega \leq 23$  meV, as shown in Fig. 11 (upper panel). This gap is even more pronounced than in the [110] direction of Cu and Ni due to the higher longitudinal sound velocity for the Fe[111] direction. There are now three divergent van Hove singularities from the stationary points in the bulk phonon dispersion. For energies between  $23 < \hbar\omega < 35$  meV there exists three propagating solutions for bulk phonons as can be seen from Fig. 10. In analogy with the fcc(110) surface, two of these solutions will exhibit complex wavevectors for phonon energies within the pseudo band gap. These complex solutions give rise to evanescent phonons localized at the surface which form vibrational resonances. This is illustrated in the surface density of states in Fig. 11 (lower panel).

In calculating the surface phonon density of states the effects of the loss of coordination of atoms on the force constants in the surface region are obtained as before by a simple truncation of the interlayer forces. The phonon density of states  $g(\omega)$  projected on the outermost surface layer shows no divergent van Hove singularities as expected from the discussion in Section 3. Two sharp resonances are found in the pseudo band gap at

19.7 and 21.3 meV (Fig. 11, lower panel). The lower lying resonance is found to be mainly localized on the first and second layer with a width of about 0.9 meV. This can be compared to the Ni(110) surface where the width of the resonance is about 3.5 meV. The higher lying resonance is found to be localized on the second and third layers. Recent electron energy loss measurements<sup>24</sup> on the Fe(111) surface are found to be in excellent agreement with these results based on surface lattice dynamics. The observed energy loss spectrum with a resonant structure at 21 meV and its comparison to the dipole projected density of states are shown in Fig. 12.

### 7. Summary

A new kind of surface vibrational resonance is shown from surface lattice dynamics to exist on surfaces having a pseudo band gap in the bulk phonon density of states. The surface splits off a mode from a region of high density of states into a pseudo band gap region where the density of states is largely depleted. This behavior is illustrated for phonons having a surface component of the wavevector along the  $\bar{r}\bar{x}$  direction in the SBZ of the (110) surfaces of Cu and Ni, and for longitudinal phonons propagating normal to the (111) surface of Fe. In these cases, the pseudo band gap is a geometric structure effect caused by the particular coordination of the atoms, which leads to higher Fourier components in the bulk phonon dispersion relations.

At the  $\bar{r}$ -point the resonance is dipole active and has been observed by EELS on the (110) surface of Cu and Ni. From these observations it has been possible to obtain information on the surface interlayer force constants. In particular, the positions of the loss peak on Cu and Ni can be reproduced with the same values for the interlayer force constants at the surface as in the bulk. Along the  $\bar{r}\bar{x}$  direction in the SBZ the

resonance makes an avoided crossing with a resonance derived from the  $S_7(\bar{X})$  surface phonon. This novel behavior should be possible to observe by inelastic electron or He scattering at large parallel wavevector transfers.

Finally, this analysis suggests in general that this type of surface vibrational resonance should be observable not only by inelastic electron dipole scattering but by other surface spectroscopies, such as inelastic He scattering, on a variety of surfaces at points in the SBZ where a bulk phonon dispersion is non-monotonic and consequently has a pseudo band gap. The origin of these effects is directly related to the geometric structure of the surface.

ACKNOWLEDGEMENTS

It is a pleasure to thank Mark Stiles and John Wilkins for stimulating discussions during the course of this work. Support of this research by the Office of Naval Research, under Contract No. N00014-81-K-0505 and No. N00014-82-K-0576, and the Swedish Natural Science Research Council is gratefully acknowledged.

APPENDIX

In this Appendix it is shown how the transfer matrix method proposed by Lee and Joannopoulos<sup>13</sup> can be applied to the calculation of surface vibrational density of states. The method is illustrated for the surface lattice dynamics problem of longitudinal phonons propagating normal to a fcc(110) surface. Furthermore, this method justifies the choice of the ansatz for the scattered waves in Eqs. (9) and (14).

The first step in this method is to form principal layers, here labelled by an integer  $n$ ,  $n=1,2,\dots$ , from the layers of atoms parallel to the surface such that the dynamical matrix only introduces interactions between displacement fields in nearest neighboring principal layers. In the present case two layers form a principal layer. The column vector  $W_n$  denotes displacement fields in the principal layer  $n$ ,

$$W_n(i) = w_{2n+i-2}, \quad i = 1, 2. \quad (A1)$$

In terms of these column vectors  $W_n$  the eigenvalue problem for the bulk layers can be written as,

$$(z - D_{00})W_n - D_{01}W_{n+1} - D_{01}^+W_{n-1} = 0, \quad n = 1, 2, \dots, \quad (A2)$$

and the corresponding equation for the surface layers is given by,

$$(z - D_{s00})W_1 - D_{01}W_2 = 0. \quad (A3)$$

Here  $z = \omega^2$  and  $D_{00}$ ,  $D_{01}$  and  $D_{s00}$  are  $(2 \times 2)$  dynamical submatrices formed from the full dynamical matrix  $D(L,L')$  which can be obtained directly from Eqs. (1) and (7).  $D_{00}(i,j) = D(2L+i-2, 2L+j-2)$ ,  $D_{01}(i,j) = D(2L+i-2, 2L+j)$ ,  $L$  denotes a bulk layer, and  $D_{s00}(i,j) = D(i,j)$ . For instance,  $D_{01}$  is given by,

$$D_{01} = \frac{\alpha}{M} \begin{pmatrix} 1 & 0 \\ 1 & 1 \end{pmatrix}. \quad (A4)$$

Equation (A2) shows explicitly that there are only interactions between displacement fields in nearest neighboring principal layers. Since  $D_{01}^{-1}$  exists  $W_{n+1}$  can be directly expressed in terms of the two preceding column vectors  $W_n$  and  $W_{n-1}$  by a simple rearrangement of Eq. (A2) as,

$$W_{n+1} = D_{01}^{-1}(z - D_{00})W_n - D_{01}^{-1}D_{01}^+W_{n-1}, \quad n = 2, 3, \dots \quad (A5)$$

This equation shows that it is possible to construct a matrix  $T(z)$  which relates the displacement fields in two principal layers  $n+2$  and  $n+1$  to the corresponding fields in the two preceding principal layers  $n$  and  $n-1$ ,

$$\begin{pmatrix} W_{n+2} \\ W_{n+1} \end{pmatrix} = T(z) \begin{pmatrix} W_n \\ W_{n-1} \end{pmatrix}, \quad (A6)$$

The matrix  $T(z)$  is the transfer matrix and is given by the product of the following two matrices,

$$T(z) = \begin{pmatrix} D_{01}^{-1}(z - D_{00}) & -D_{01}^{-1}D_{01}^+ \\ 1 & 0 \end{pmatrix} \begin{pmatrix} D_{01}^{-1}(z - D_{00}) & -D_{01}^{-1}D_{01}^+ \\ 1 & 0 \end{pmatrix} \quad (A7)$$

By iterating Eq. (A6), a displacement field in any principal layer can be determined from their values on the surface layers as,

$$\begin{pmatrix} W_{n+2} \\ W_{n+1} \end{pmatrix} = T^n(z) \begin{pmatrix} W_2 \\ W_1 \end{pmatrix}. \quad (A8)$$

Equation (A3) for  $W_2$  and  $W_1$  gives only 2 equations for 4 displacement fields and are not sufficient to determine  $W_2$  and  $W_1$ . Further restrictions are found by introducing the appropriate boundary conditions. That can be done by analyzing the eigenvalues and eigenvectors of the dynamical matrix.

For the bulk layers the solution to Eq. (A2) is given by translational symmetry as plane waves,

$$w_n = \begin{pmatrix} e^{i2n\pi\zeta} \\ e^{i(2n-1)\pi\zeta} \end{pmatrix}, \quad (A9)$$

where the reduced wavevector  $\zeta$  satisfies the bulk dispersion relation

$\omega^2 = \omega_0^2(\sin^2(\pi\zeta/2) + \sin^2(\pi\zeta))/2$  as given by Eq. (3) in Section 3. In terms of the variable  $\lambda = e^{i\pi\zeta}$  this dispersion relation is equivalent to a polynomial of degree 4 in  $\lambda$  and has accordingly 4 roots  $\lambda_k$ ,  $k=1,2,3,4$ .

The eigenvectors  $v_k(z)$  of  $T(z)$  can now be directly formed from these plane wave solutions,

$$v_k(z) = \begin{pmatrix} \lambda_k^3 \\ \lambda_k^2 \\ \lambda_k \\ 1 \end{pmatrix} \quad (A10)$$

and the associated eigenvalue for  $v_k(z)$  is given by  $\lambda_k^4$  and  $T(z)v_k = \lambda_k^4 v_k$ . The eigenvalues are distinct away from the critical points,  $d\omega/d\zeta = 0$ , and the corresponding eigenvectors span the 4-dimensional space of displacement fields of two adjacent principal layers. Thus  $w_2$  and  $w_1$  can then be simultaneously expanded in terms of

$v_k$ ,

$$\begin{pmatrix} w_2 \\ w_1 \end{pmatrix} = \sum_{k=1}^4 c_k v_k. \quad (A11)$$

This equation and Eq. (A8) give directly that the displacement field for any principal layer can be expressed as,

$$\begin{pmatrix} w_{2n+2} \\ w_{2n+1} \end{pmatrix} = \sum_{k=1}^4 c_k \lambda_k^{4n} v_k, \quad n=0,1,2,\dots, \quad (A12)$$

or in terms of the displacement field  $w_L$  for a layer  $L$ ,

$$w_L = \sum_{k=1}^4 \tilde{c}_k e^{i\pi\xi_k L}, \quad (A13)$$

where  $\tilde{c}_k = c_k e^{-i2\pi\xi_k L}$ . This form of solution in Eq. (A13) justifies the ansatz made in Eqs. (9) and (14) in Section 3. The solution corresponding to scattered wave can be found by imposing the outgoing boundary conditions as discussed in Section 3. This restricts the solutions to depend on two parameters. These two parameters can then be determined from the two equations for the surface layers.

A more convenient way to evaluate the vibrational density of states  $g(\omega, \{n_L\})$  than using the scattered wave solutions appearing in Eq. (A13) is to determine first the resolvent matrix (a Green function)  $U(L, L'; z)$  associated with the dynamical matrix  $D(L, L')$ . This resolvent is defined by,

$$\{[z\delta(L, L'') - D(L, L'')]U(L'', L'; z) = \delta(L, L'), \quad (A14)$$

and the vibrational density of states is given by,

$$g(\omega, \{n_L\}) = \frac{2\omega}{\pi} \operatorname{Im} \sum_{L, L'} n_L U(L, L'; (\omega + i0^+)^2) n_{L'}. \quad (A15)$$

The transfer matrix approach can now be applied by considering the resolvent (2x2) submatrices  $U_{n, n'}(z)$  with respect to the principal layers and they are defined as,

$$U_{n, n'}(i, j; z) = U(2n-L+i, 2n'+L-j; z), \quad i, j = 1, 2. \quad (A16)$$

To obtain the vibrational density of states for the surface layers it is sufficient to evaluate  $U_{1, 1}(z)$ . The resolvent matrix element  $U_{n, 1}(z)$  satisfies the same equations as  $W_n$ , Eq. (A2), except at the surface layers where the equations have an inhomogenous term,

$$(z - D_{s00})U_{1,1}(z) - D_{01}U_{2,1}(z) = 1 \quad (A17)$$

Similar to the construction of  $W_n$ ,  $U_{n,1}(z)$  can be constructed from

$U_{1,1}(z)$  and  $U_{2,1}(z)$  by iterating the transfer matrix,

$$\begin{pmatrix} U_{2n+2,1}(z) \\ U_{2n+1,1}(z) \end{pmatrix} = T^n(z) \begin{pmatrix} U_{2,1}(z) \\ U_{1,1}(z) \end{pmatrix}. \quad (A18)$$

Some care is needed to get the correct physical Riemann sheet of the resolvent as a function of  $z$ . On this sheet  $U_{n,1}(z)$  has to be decaying with  $n$  when imparting a small positive imaginary part is to  $\omega$ ,  $z = (\omega + i\epsilon)^2$ . Such a decay is evidently achieved by expanding the two column vectors of  $U_{2,1}(z)$  and  $U_{1,1}(z)$  simultaneously in terms of those eigenvectors with  $|\lambda_k| < 1$ . This point and the fact that for complex  $z$  the eigenvectors are divided evenly into two classes  $|\lambda_k| < 1$  and  $|\lambda_k| > 1$ , respectively, were shown in detail for the general case in the original work by Lee and Joannopoulos.<sup>13</sup> Let  $k=1,2$  label the two eigenvectors with  $|\lambda_k| < 1$  and introduce the two associated  $(2 \times 2)$  matrices,

$$\begin{aligned} W_U(i,j) &= V_j(i) \\ W_L(i,j) &= V_j(i+2). \end{aligned} \quad (A19)$$

The expansion of the two submatrices of the resolvent in these two eigenvectors now becomes,

$$\begin{pmatrix} U_{2,1}(z) \\ U_{1,1}(z) \end{pmatrix} = \begin{pmatrix} W_U A \\ W_L A \end{pmatrix} \quad (A20)$$

where the coefficients in the expansion forms a  $(2 \times 2)$  matrix  $A$ . These two resolvents are now specified by 4 parameters. The 4 surface layer equations in Eq. (A17) for  $U_{1,1}(z)$  and  $U_{2,1}(z)$  will now completely determine these parameters. This can be done by first eliminating the

matrix A from Eq. (A20).

$$U_{2,1}(z) = W_U W_L^{-1} U_{1,1}(z). \quad (A21)$$

Furthermore, by inserting this expression for  $U_{2,1}(z)$  into Eq. (A17) a simple linear matrix equation is obtained for  $U_{1,1}(z)$  which can be solved by a matrix inversion,

$$U_{1,1}(z) = (z - D_{s00} - D_{01} W_U W_L^{-1})^{-1}. \quad (A22)$$

Thus for every frequency  $\omega$  the vibrational density of states can be evaluated from Eqs. (A15) and (A22) by diagonalization of a  $(4 \times 4)$  complex matrix and by inversion of two  $(2 \times 2)$  matrices.  $U_{1,1}(z)$  will have simple poles at those frequencies corresponding to localized vibrational modes at the surface. Similarly, the resonances appear as poles in the complex frequency plane but not on the physical Riemann sheet of  $U_{1,1}(z)$ . However, the other Riemann sheets of  $U_{1,1}(z)$  should be possible to construct from other choices for the eigenvectors in Eq. (A19).

REFERENCES

<sup>t</sup>Permanent address: Institute of Theoretical Physics, Chalmers University of Technology, S-412 96 Göteborg, Sweden.

\*Present address: IBM, T.J. Watson Research Center, Yorktown Heights, NY 10598.

1. S. Lehwald, J.M. Szeftel, H. Ibach, T.S. Rahman, and D.L. Mills, Phys. Rev. Lett. 50, 518 (1983); M. Rocca, S. Lehwald, H. Ibach, and T.S. Rahman, Surf. Sci. 138, 1123 (1984).
2. R.B. Doak, U. Harten, and J.P. Toennies, Phys. Rev. Lett. 51, 578 (1983).
3. M. Cates and D.R. Miller, J. Electron Spectrosc. Relat. Phenom. 30, 157 (1983).
4. M.-L. Xu, B.M. Hall, S.Y. Tong, M. Rocca, H. Ibach, S. Lehwald, and J.E. Black, Phys. Rev. Lett. 54, 1171 (1985).
5. V. Bortolani, A. Franchini, F. Nizzoli, and G. Santoro, Phys. Rev. Lett. 52, 429 (1984).
6. S. Andersson, B.N.J. Persson, M. Persson, and N.D. Lang, Phys. Rev. Lett. 52, 2073 (1984).
7. J.A. Stroscio, M. Persson, S.R. Bare, and W. Ho, Phys. Rev. Lett. 54, 1428 (1984).
8. For a recent compilation of data see: Y. Gauthier, R. Baudoing, Y. Joly, C. Gaubert, and J. Rundgren, J. Phys. C 17, 4547 (1984).
9. V. Bortolani, A. Franchini, N. Garcia, F. Nizzoli, and G. Santoro, Phys. Rev. B 28, 7358 (1983).
10. E.C. Svensson, B.N. Brockhouse, and J.M. Rowe, Phys. Rev. 155, 619 (1967).
11. R.J. Birgenau, J. Cordes, G. Dolling, and A.D.B. Woods, Phys. Rev. 136, A1359 (1964).

References cont.

12. V.J. Minkiewicz, G. Shirane, and R. Nathans, Phys. Rev. 162, 528 (1967).
13. D.H. Lee and J.D. Joannopoulos, Phys. Rev. B 23, 4997 (1981).
14. R.E. Allen, G.P. Alldredge, and F.W. deWette, Phys. Rev. B 4, 1661 (1971).
15. J.A. Stroscio, Ph.D. thesis, Cornell University, 1986. See also M. Persson, J.A. Stroscio, and W. Ho, Proceedings of the 4th International Conference on Vibrations at Surfaces, Lake Districts, England, J. Electron Spectrosc. Relat. Phenom. (to be published).
16. J.A. Stroscio, S.R. Bare, and W. Ho, Surf. Sci. 148, 499 (1984).
17. W. Ho, R.F. Willis, and E.W. Plummer, Phys. Rev. Lett. 40, 1463 (1978); Phys. Rev. B 21, 4202 (1980).
18. A.A. Maradudin, E.W. Montroll, G.H. Weiss, and I.P. Ipatore, Lattice Dynamics in the Harmonic Approximation, 2nd edition (Academic, New York, 1981).
19. U. Fano, Phys. Rev. 124, 1866 (1961).
20. H. Ibach and D.L. Mills, Electron-Energy-Loss Spectroscopy and Surface Vibrations (Academic, New York, 1982).
21. M. Persson, Phys. Scr. 29, 181 (1984).
22. S. Andersson and B.N.J. Persson, Phys. Rev. Lett. 50, 2028 (1983).
23. M.W. Finnis and V. Heine, J. Phys. F4, L37 (1974); U. Landmann, R.N. Hill, and M. Mostoller, Phys. Rev. B 21, 448 (1980); R.N. Barnett, U. Landmann, and C.L. Cleveland, Phys. Rev. Lett. 51, 1359 (1983).
24. J.A. Stroscio, M. Persson, C.E. Bartosch, and W. Ho, Phys. Rev. (to be published).
25. J.A. Stroscio, M. Persson, and W. Ho (to be published).

Figure Captions

Fig. 1: Electron energy loss spectra of the clean (110) surfaces of Cu and Ni. The spectra were recorded in the specular direction at 300 K. The sharp peaks observed at 20 and 24 meV, for Cu and Ni respectively, correspond to surface vibrational resonances.

Fig. 2: Longitudinal bulk phonon dispersion relations in the [110], [111] and [100] directions of Cu and Ni. The data from inelastic neutron scattering are compared with results from a nearest neighbor central force constant model. The interlayer distance is  $d$ .

Fig. 3: Structure of fcc crystals in the [110] and [100] directions. (a) Top view of atoms of the (110) surface together with the crystallographic directions. The (110) surface Brillouin zone is depicted in (b). The coordination of atoms in the bulk layers normal to the surface are shown for (c) the [110] and (d) the [100] directions.

Fig. 4: The density of states  $g(\omega)$  for longitudinal phonons projected on bulk and surface layers for Ni. The results for  $g(\omega)$  in the [110], [111] and [100] crystal directions have been calculated using the same force constant model as in Fig. 2.

Fig. 5: Calculated electron energy loss function  $I_1(\omega)/I_0$  for Ni(110) at 300 K.  $I_0$  is the maximum intensity of the elastic peak in the energy loss spectrum. Only the two outermost surface layers are assumed to be dipole active and the total effective charge  $e^*_{tot}$  has been adjusted to  $0.039e$  ( $e$  is the free electron charge) in order to reproduce the measured loss in Fig. 1. The instrumental resolution has been introduced by a Gaussian broadening of 4 meV.

Fig. 6: Sensitivity of  $g(\omega)$  to different models for the surface force constants and the effective charge fields. Upper panel shows the results for different values of the surface interlayer force constant  $\alpha_s$  relative to the bulk interlayer force constant  $\alpha$ . The relative motion of the two outermost layers has been used in obtaining the dipole active projection for  $g(\omega)$ . Lower panel shows the results for different choices of the effective charges  $(e_1^*, e_2^*, e_3^*, e_4^*)$  of the four outermost surface layers,  $e_{tot}^* = 1$  when  $\alpha_s = \alpha$ .

Fig. 7: Dispersion of bulk phonons in the [110] direction of Ni and the corresponding surface phonon density of states  $g(\omega)$  at  $\xi = k_x a / \sqrt{2\pi} = 0.6$ . The left panel shows the two branches, an upper "U" and a lower "L" branch, of the dispersion in the [110] direction (solid lines) arising from an avoided crossing between phonons polarized in the x- and z- directions, respectively. The dashed lines show the dispersion when the interaction between these two polarizations is turned off. The right panel shows the phonon density of states  $g(\omega)$  projected on the z-motion (solid line) and the x-motion (dashed line) of the outermost surface layer.

Fig. 8: Dispersion of the resonance along the  $\bar{\Gamma}\bar{X}$ -direction. The dispersion of the resonance arising from the pseudo band gap (squares) makes an avoided crossing with the dispersion of the resonance (circles) derived from the  $S_7(\bar{X})$  surface phonon. The solid lines give the maximum  $\hbar\omega_{L,max}$ ,  $\hbar\omega_{U,max}$  and minimum  $\hbar\omega_{L,min}$ ,  $\hbar\omega_{U,min}$  energies of the lower and the upper boundaries of bulk subbands, respectively. The dashed lines show

$\hbar\omega_L(\xi, \zeta=1)$  and  $\hbar\omega_U(\xi, \zeta=1)$  for phonons with a reduced wavevector  $\xi = k_z a / \sqrt{2}\pi$  where  $a$  is the lattice constant. The notation of the surface resonances  $S_1$  and  $S_7$  are taken from Ref. 14.

Fig. 9: Structure of a bcc(111) surface. The two different views of the atoms (solid circles) are defined by the indicated crystallographic directions. The atoms in (a) are enumerated according to which layer they belong with number one corresponding to the surface layer. The solid bars in the side view (b) connects nearest and next nearest neighboring atoms. The dashed circles represent atoms in an adjacent layer of atoms.

Fig. 10: Longitudinal bulk phonon dispersion in the [111] direction of Fe. The data from inelastic neutron scattering<sup>12</sup> (squares) are compared with the result from a tensor force constant model extending to second nearest neighboring atoms. The lattice constant is  $a$ .

Fig. 11: The projected density of states  $g(\omega)$  for longitudinal phonons on a bulk layer (upper panel) and the outermost surface layer (lower panel) of Fe(111).

Fig. 12: Electron energy loss spectrum of the Fe(111) surface. The spectrum was recorded in the specular direction at 300 K. The sharp peak observed at 21 meV corresponds to a surface vibrational resonance. The small, broad structure at - 60 meV is due to < 1% contamination of oxygen. The inset shows the dipole projected density of states calculated for a projection on the relative motion of the outer two surface layers and convoluted with a 4.5 meV Gaussian broadening due to instrumental resolution.

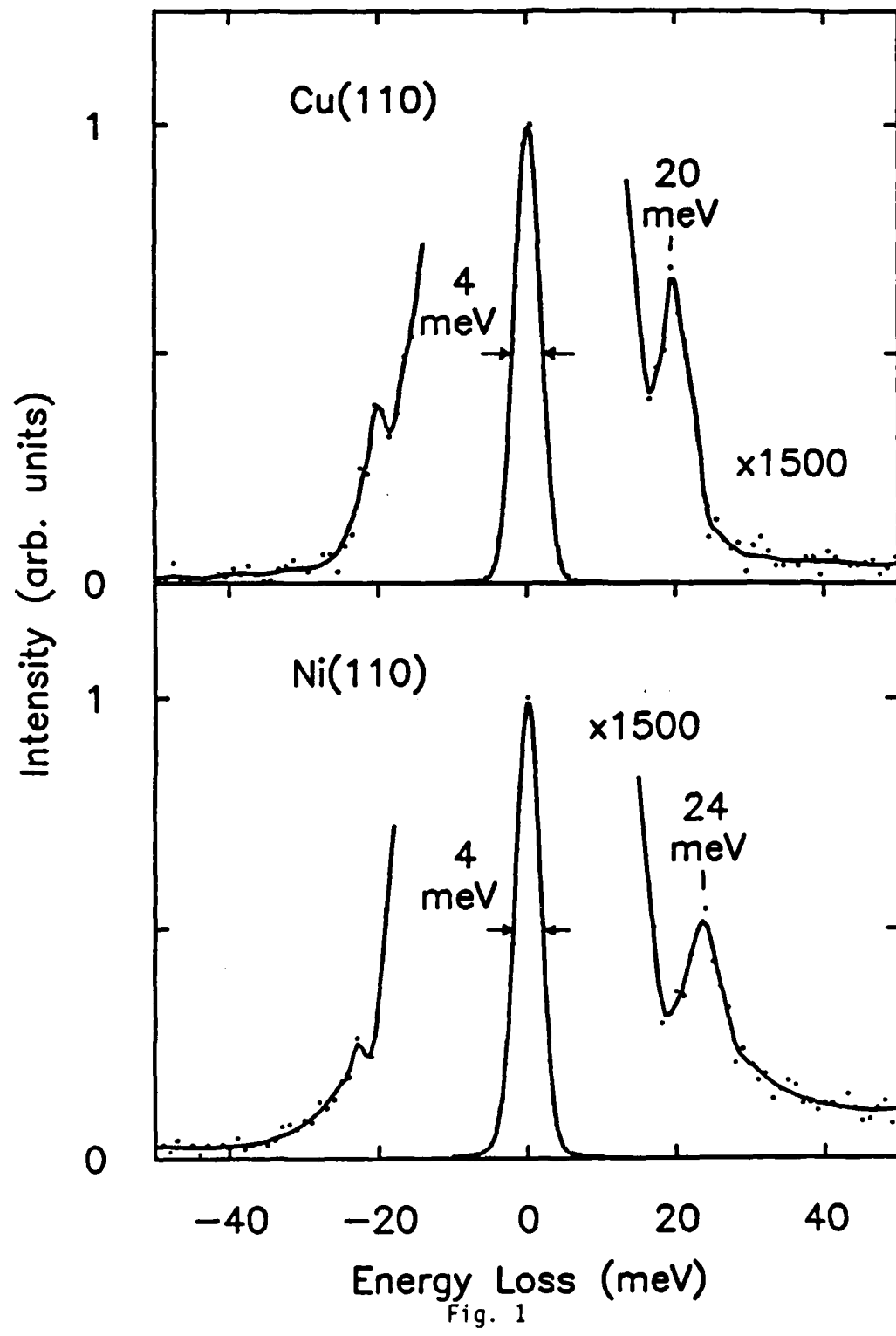


Fig. 1

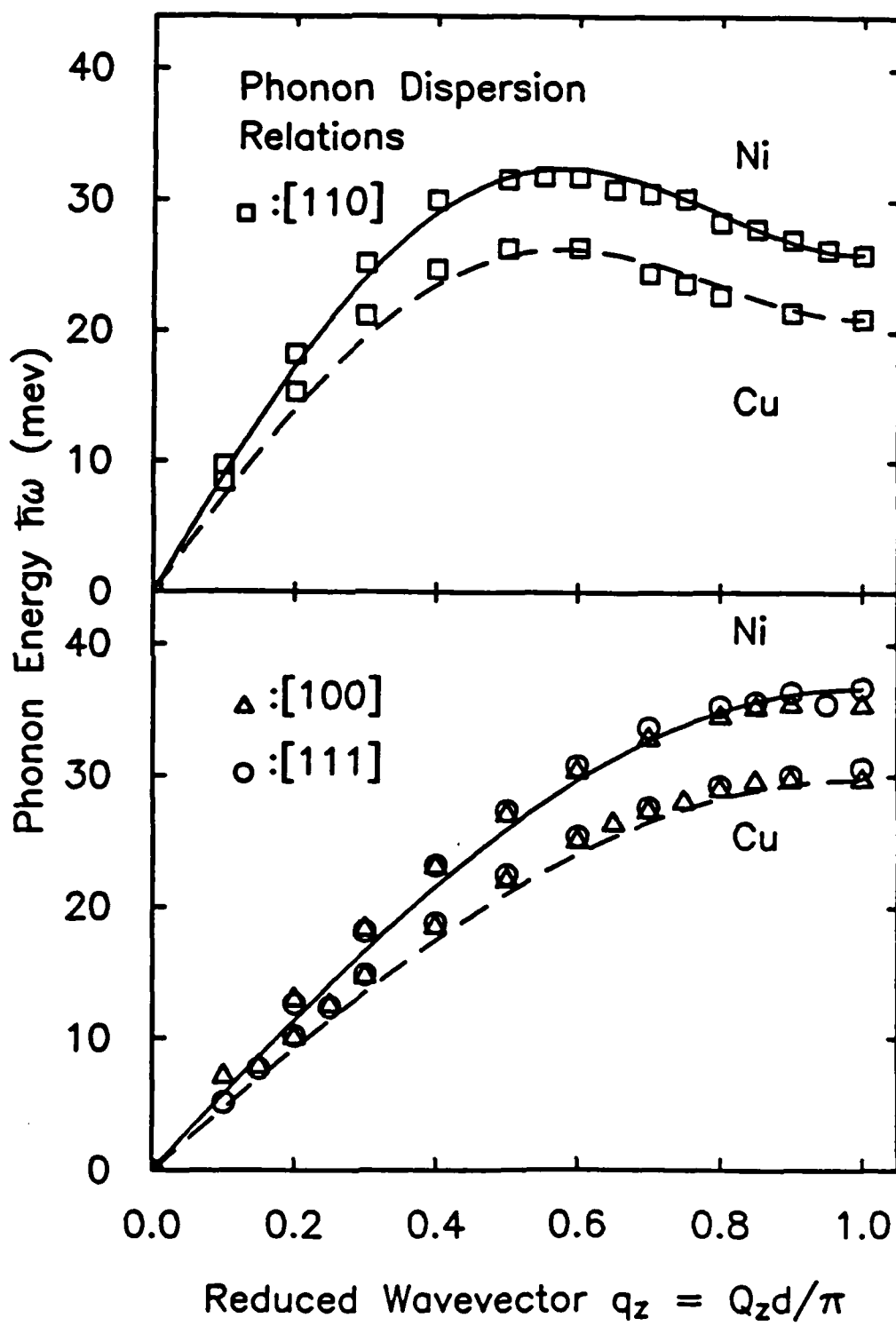


Fig. 2

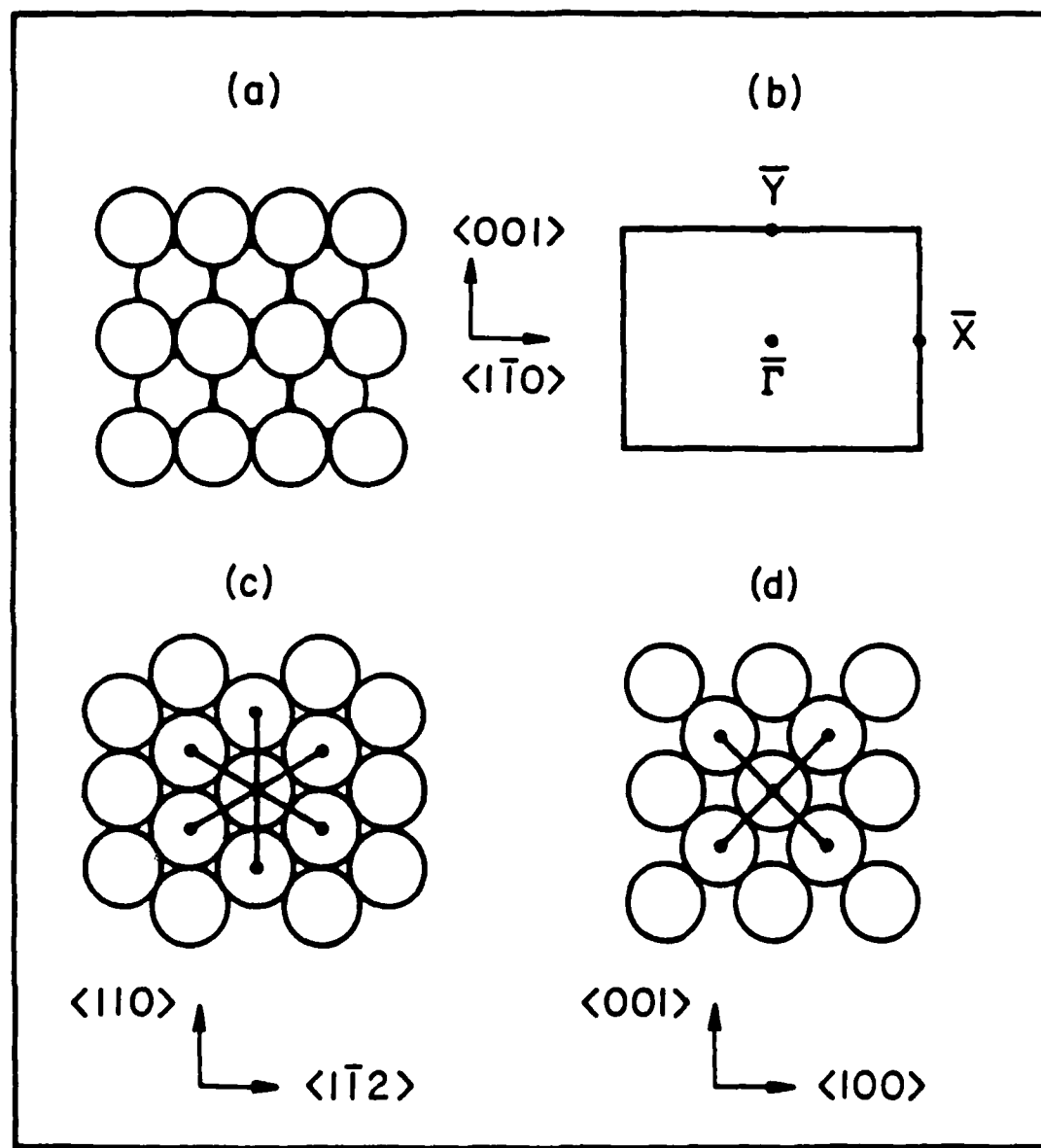


Fig. 3

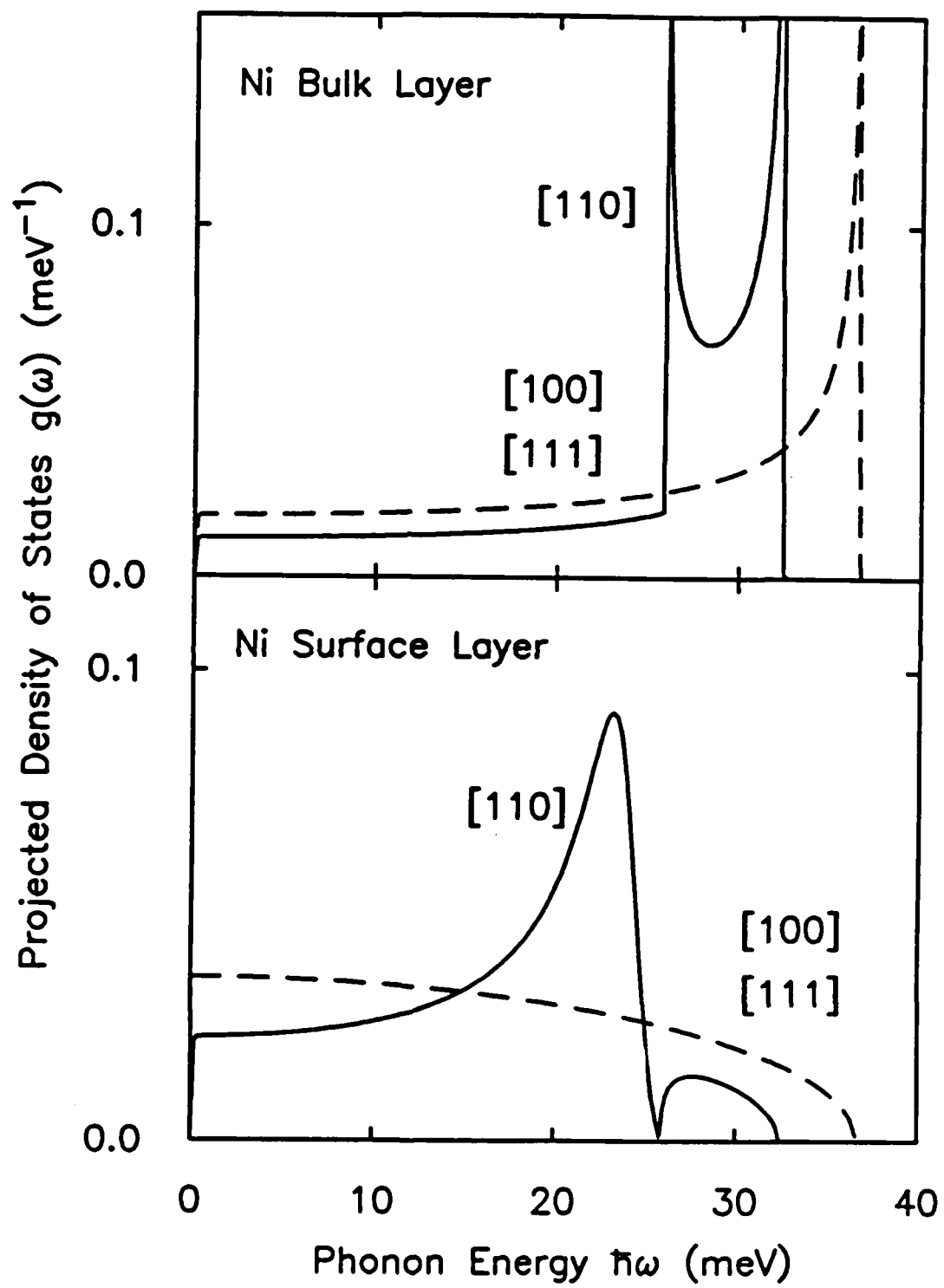


Fig. 4

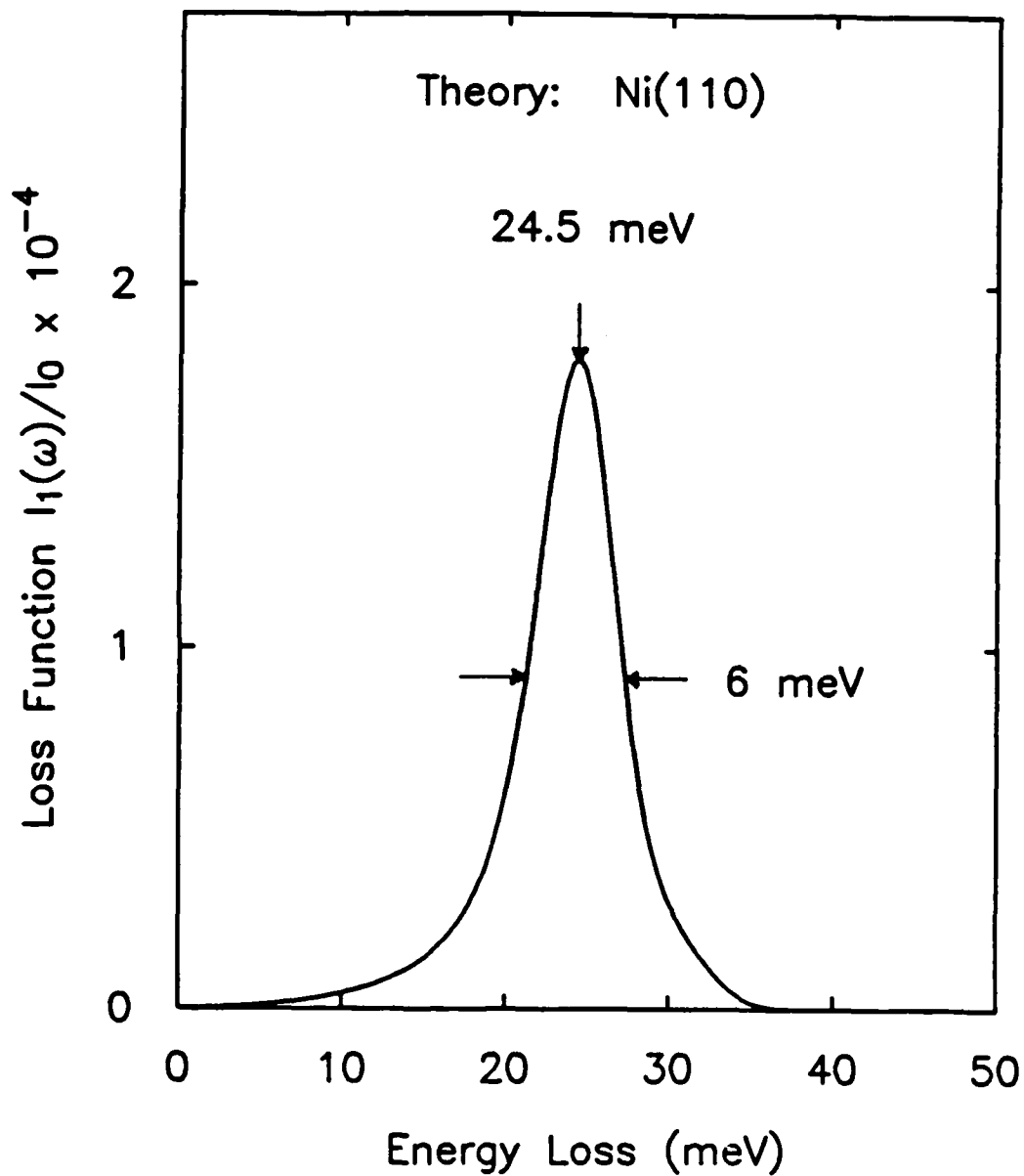


Fig. 5

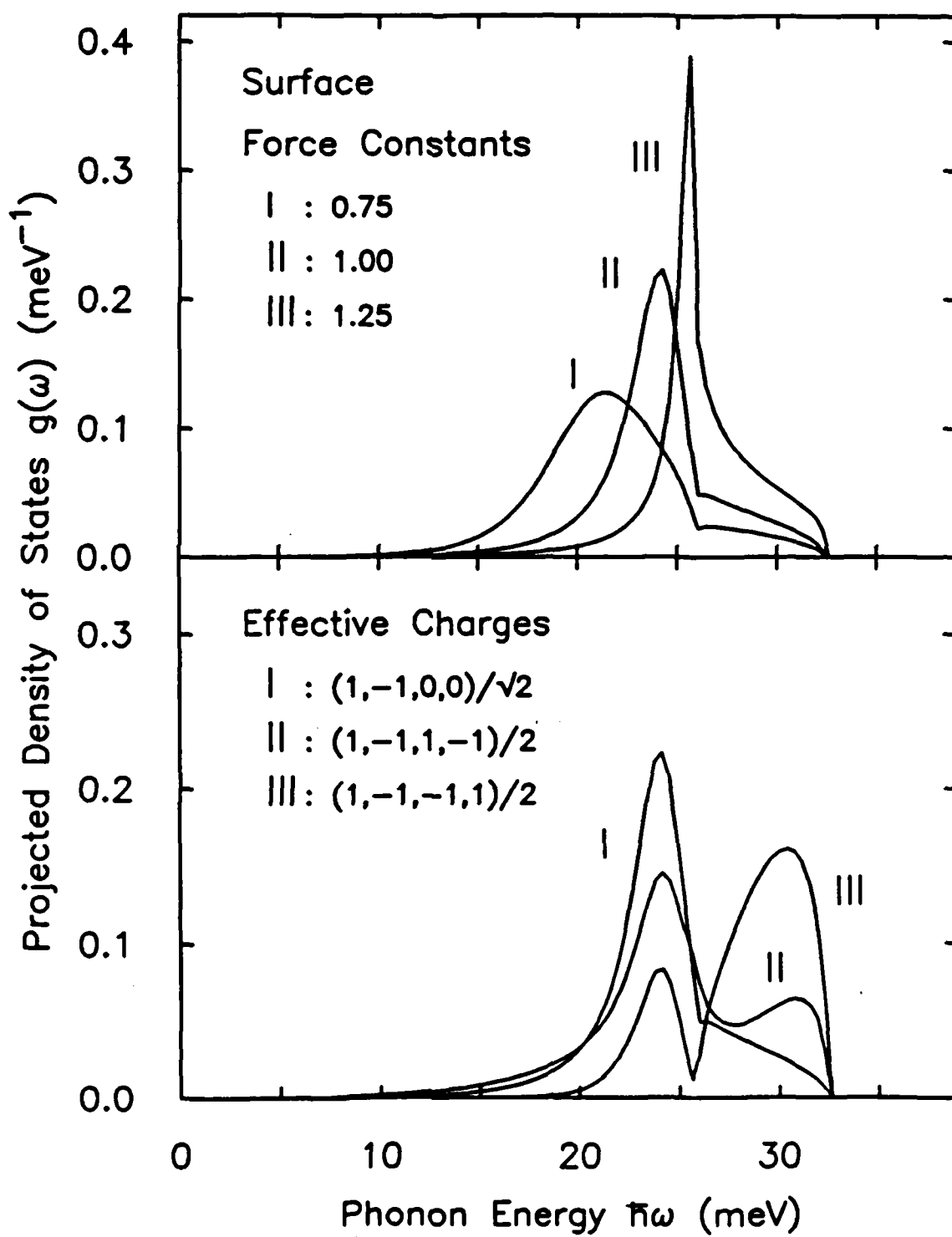


Fig. 6

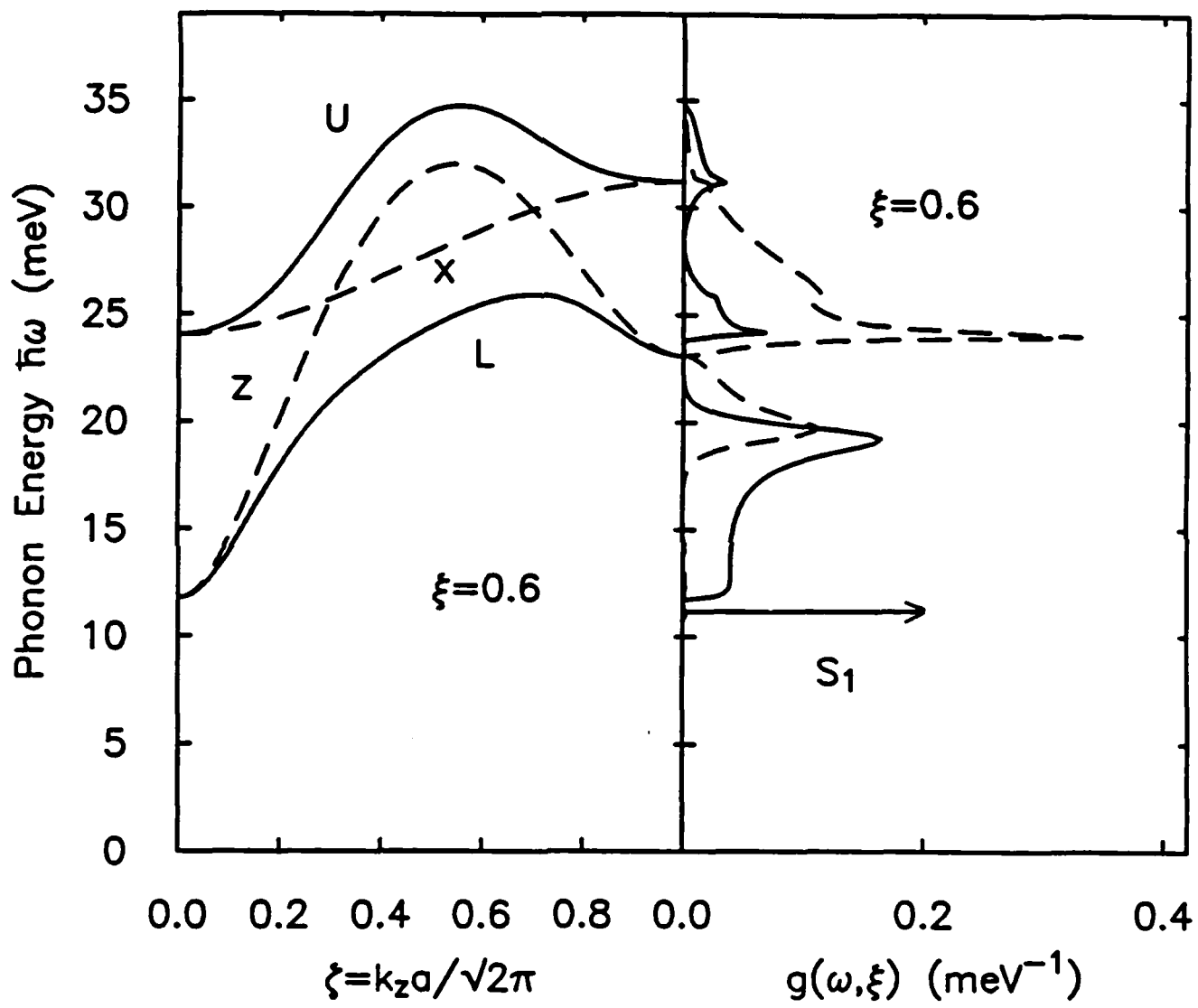


Fig. 7

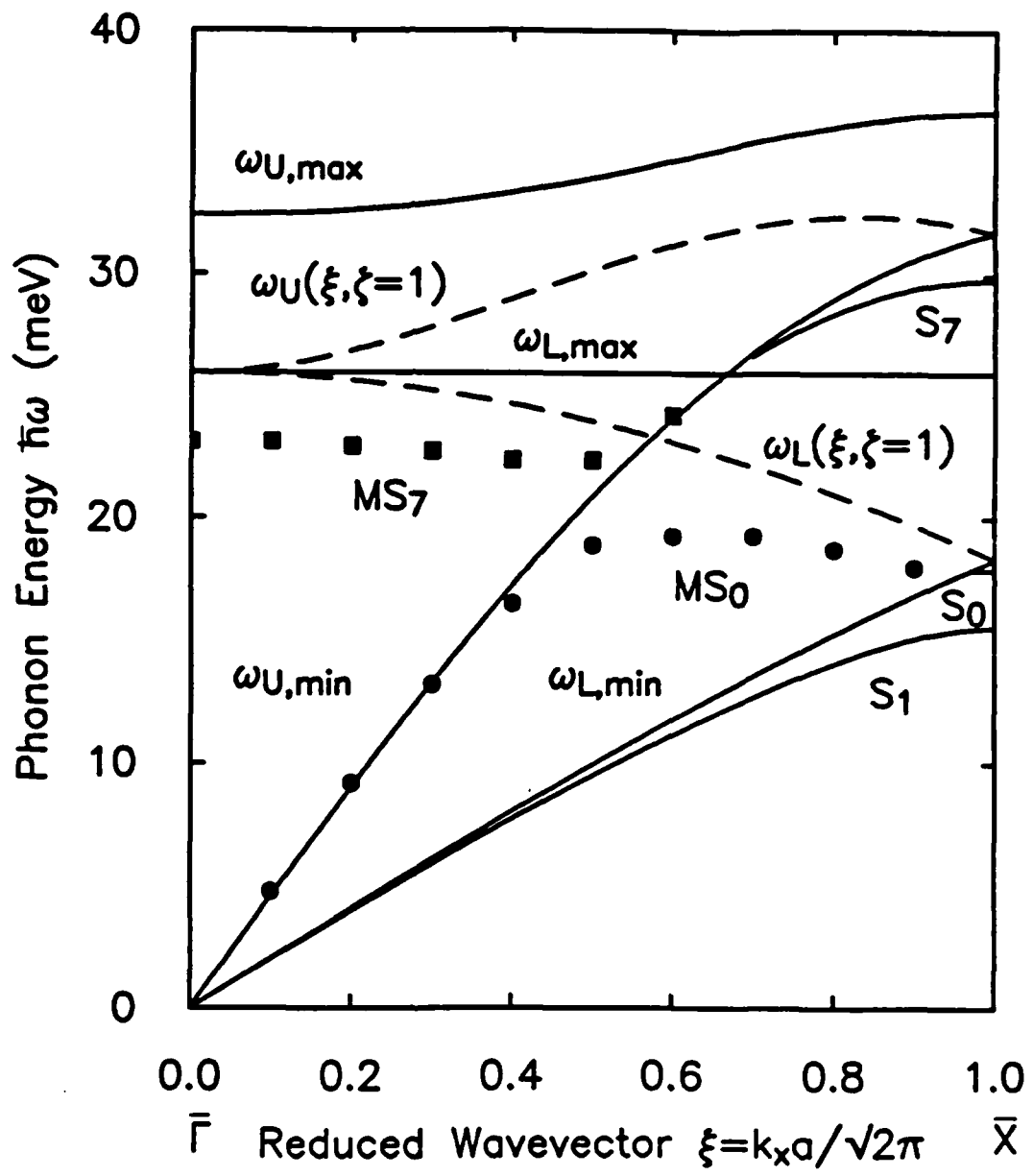


Fig. 8

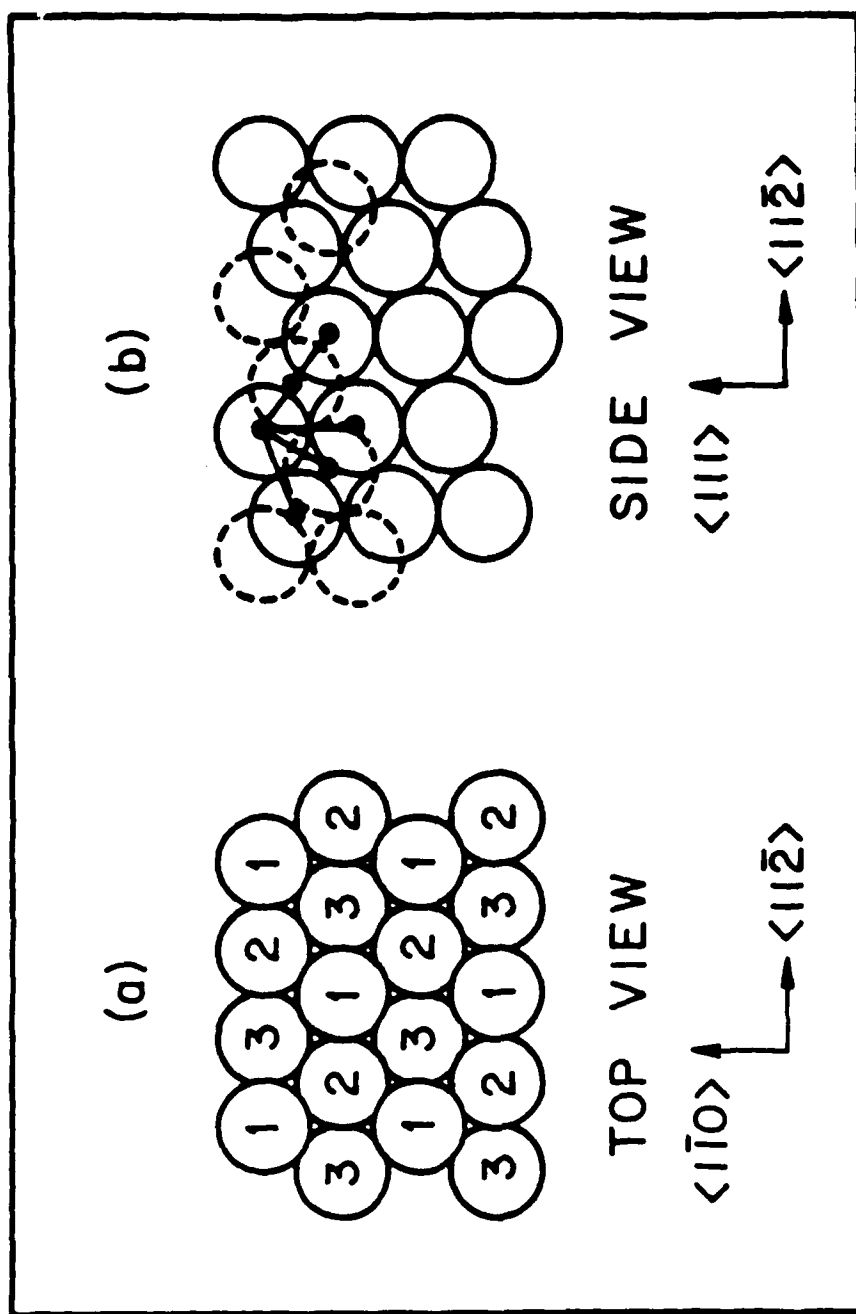


Fig. 9

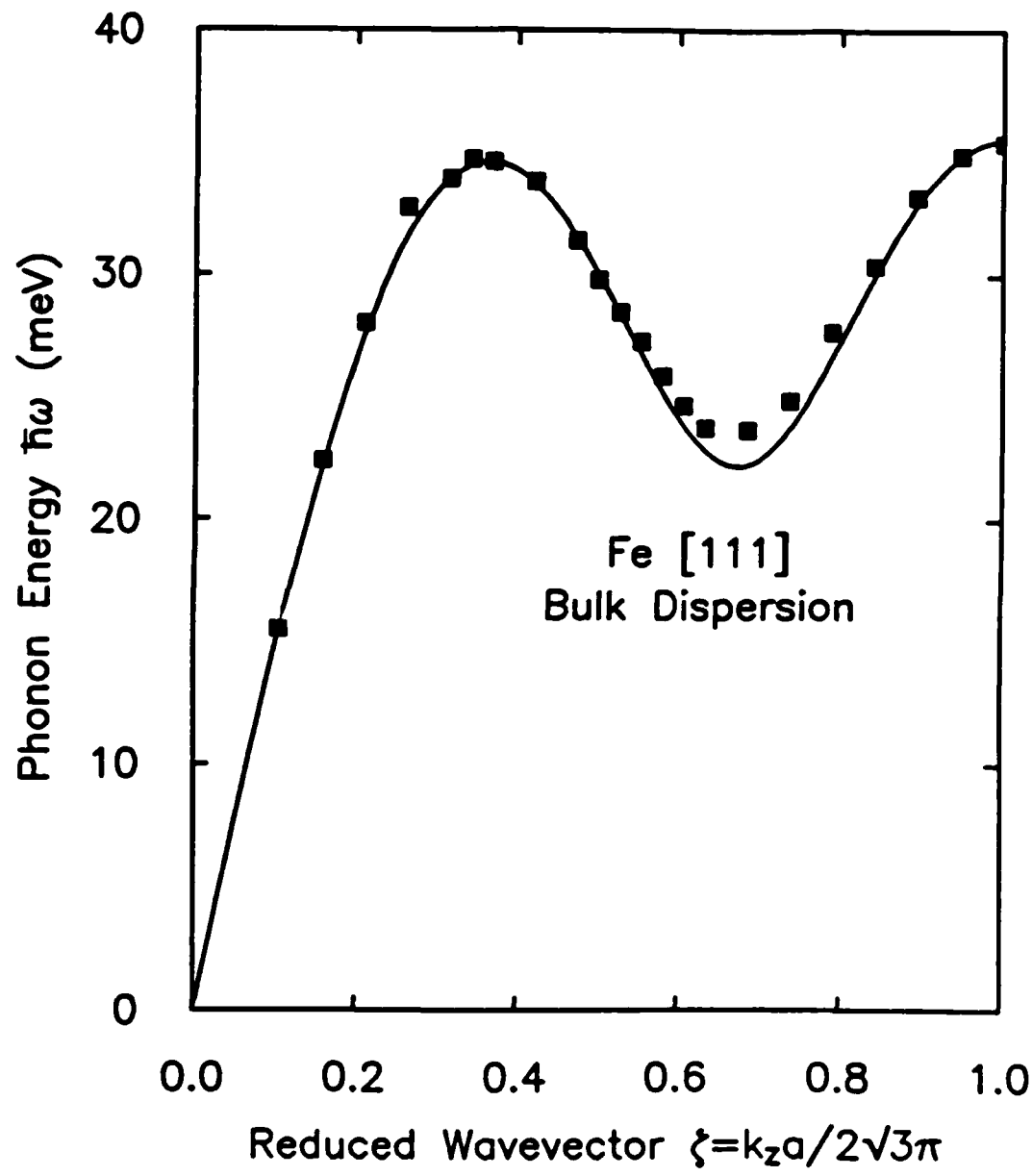


Fig. 10

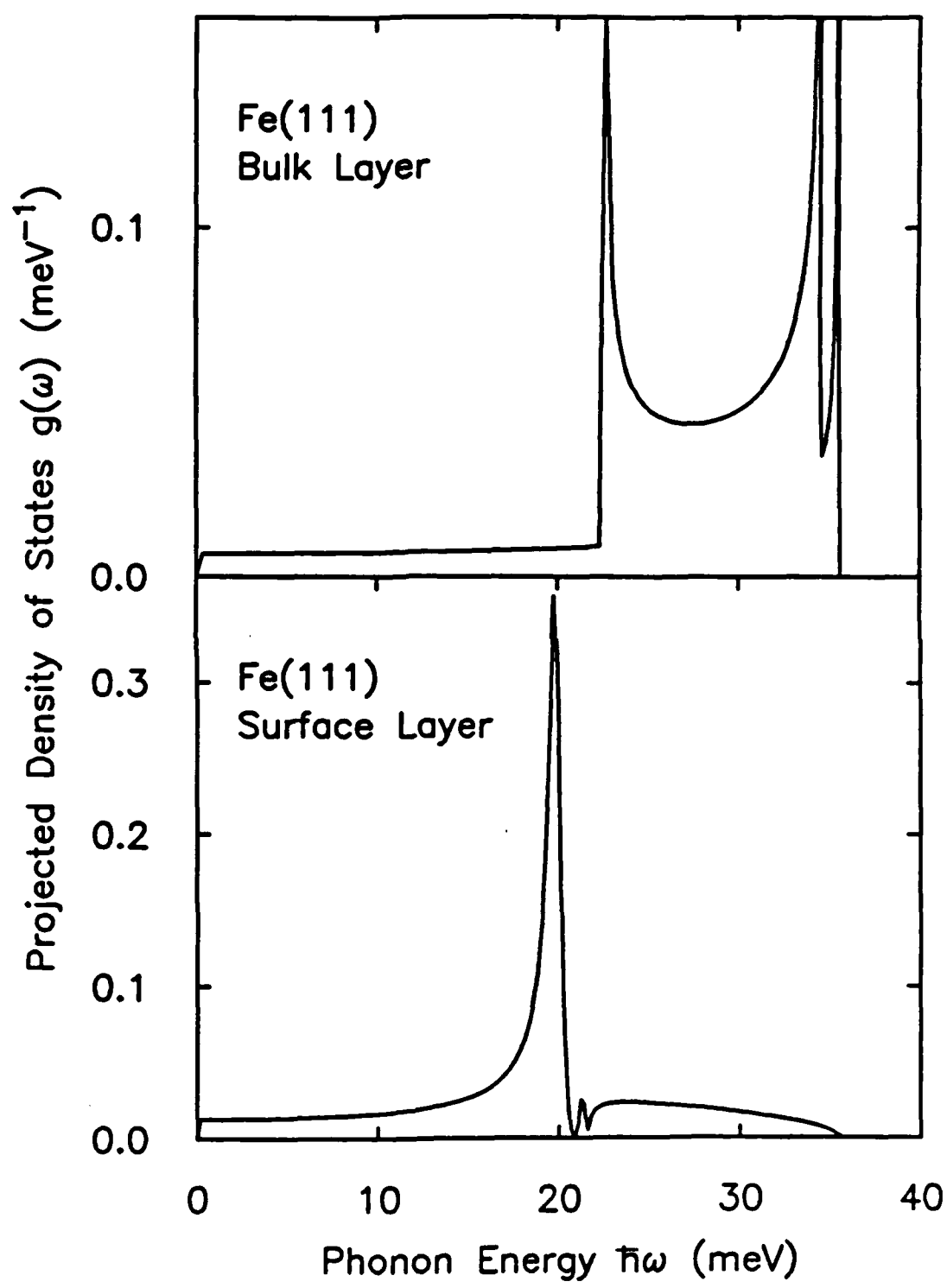


Fig. 11

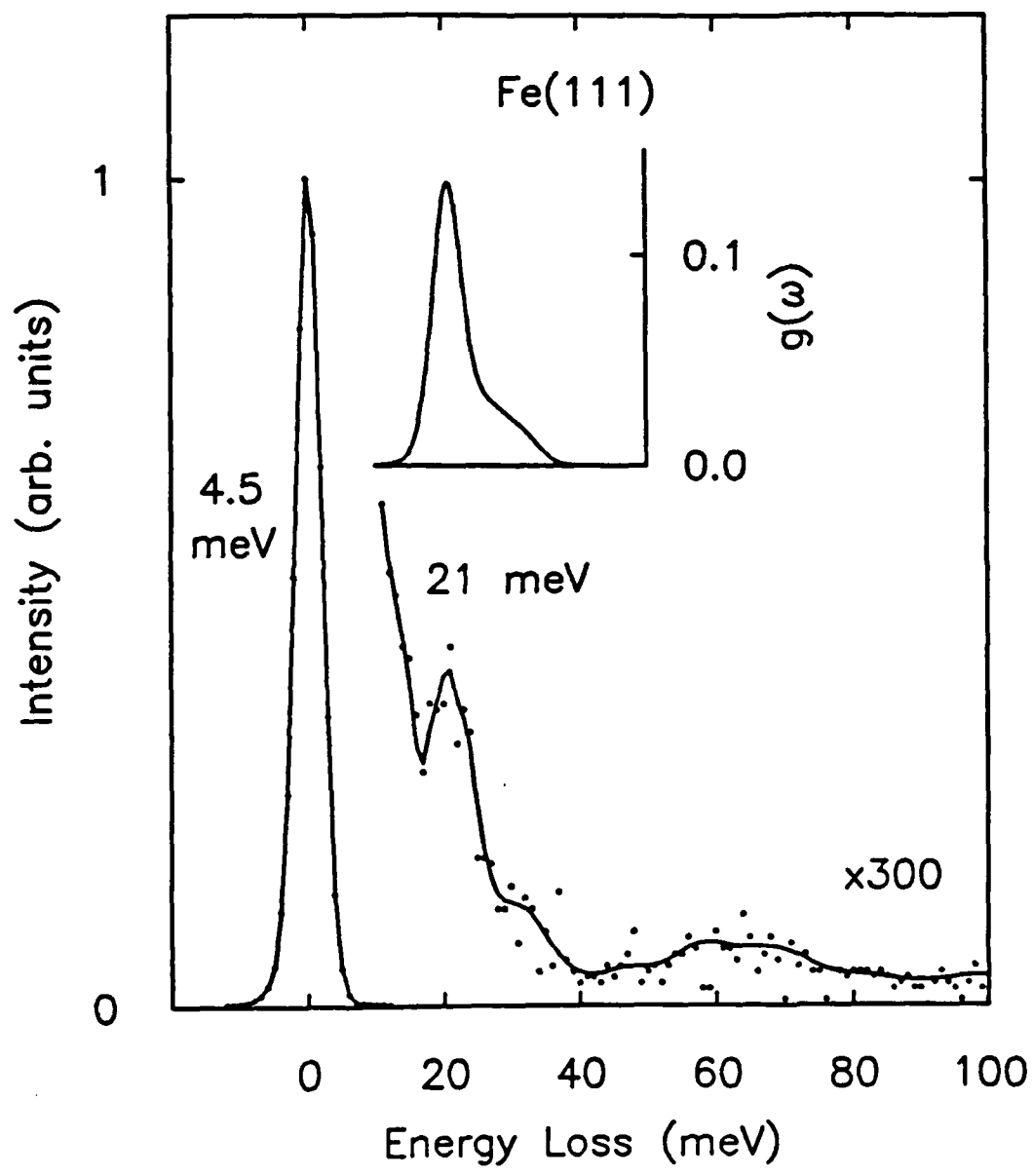


Fig. 12

END

DTIC

7 — 86